1999

A study of periodic orbits about ellipsoidal shaped bodies

Travis Arthur Becker
San Jose State University

INFORMATION TO USERS

This manuscript has been reproduced from the microfilm master. UMI films the text directly from the original or copy submitted. Thus, some thesis and dissertation copies are in typewriter face, while others may be from any type of computer printer.

The quality of this reproduction is dependent upon the quality of the copy submitted. Broken or indistinct print, colored or poor quality illustrations and photographs, print bleedthrough, substandard margins, and improper alignment can adversely affect reproduction.

In the unlikely event that the author did not send UMI a complete manuscript and there are missing pages, these will be noted. Also, if unauthorized copyright material had to be removed, a note will indicate the deletion.

Oversize materials (e.g., maps, drawings, charts) are reproduced by sectioning the original, beginning at the upper left-hand corner and continuing from left to right in equal sections with small overlaps.

Photographs included in the original manuscript have been reproduced xerographically in this copy. Higher quality 6" x 9" black and white photographic prints are available for any photographs or illustrations appearing in this copy for an additional charge. Contact UMI directly to order.

Bell & Howell Information and Learning
300 North Zeeb Road, Ann Arbor, MI 48106-1346 USA

UMI®
800-521-0600

A STUDY OF PERIODIC ORBITS ABOUT ELLIPSOIDAL SHAPED BODIES

A Thesis

Presented to

The Faculty of the Department of

Mechanical and Aerospace Engineering

San José State University

In Partial Fulfillment

of the Requirements for the Degree

Master of Science in

Aerospace Engineering

By

Travis Arthur Becker

December, 1999

APPROVED FOR THE DEPARTMENT

OF MECHANICAL AND AEROSPACE ENGINEERING

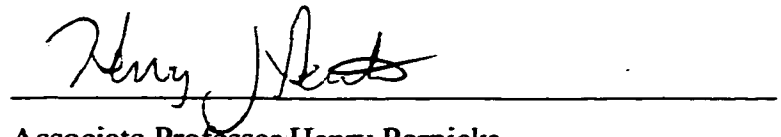

Associate Professor Henry Pernicka

Professor Patrick Hamill

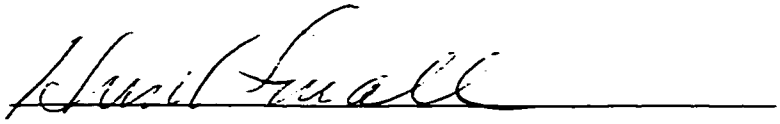

Dr. Hunt Small, Lockheed Martin Corporation

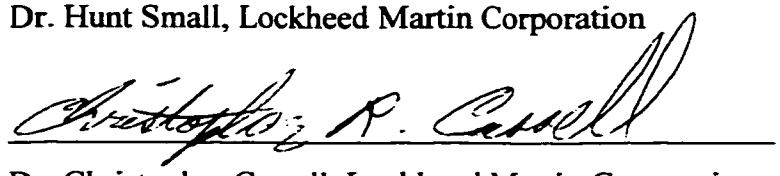

Dr. Christopher Cassell, Lockheed Martin Corporation

APPROVED FOR THE UNIVERSITY

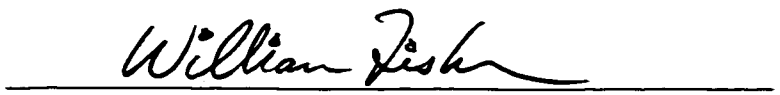

ABSTRACT

A STUDY OF PERIODIC ORBITS ABOUT ELLIPSOIDAL SHAPED BODIES

by Travis A. Becker

This thesis summarizes an investigation of periodic orbits about asteroids and comets, with a focus on polar orbits. A force model is derived assuming a triaxial ellipsoid shape for the central body, with constant density, and a constant spin rate oriented along the maximum moment of inertia axis of the body. No external perturbations are included. Several numerical studies performed on test asteroids are described. Parametric studies show the variation of the orbital elements over the course of thirty days as a function of the initial semimajor axis. Phase plots, showing eccentricity as a function of argument of periapsis on a polar plot, are developed for some of these orbits, and the nature of the plots are used as an aid to study the general trends of the orbits in question. Lagrange's Planetary Equations are used to derive the rate of change of periapsis distance as a function of mean anomaly (i.e., dr_p/dM), and the resulting periapsis plots are also used to study the orbital nature. Finally, a differential corrections method is used to produce periodic orbits based on promising orbits from these studies.

Two variations of the differential correction method are used, with initial condition estimates taken from resonance orbits about two asteroids. In addition, an orbit "conditioner" is also used to aid in convergence. The program developed produced two useful orbits. Both orbital paths remain relatively close to the surface and may be useful in mission design. A number of initial estimates did not converge, however. More study is required in this area, and a number of recommendations for future work are given.

ACKNOWLEDGMENTS

I wish to thank first and foremost my advisor, Associate Professor Henry Pernicka, for his wisdom, drive, and friendship during my graduate education at San José State. This has been an invaluable learning experience for me, and I am most grateful to him.

I also wish to thank Professor Patrick Hamill of San José State, and Drs. Chris Casselll and Hunt Small for their review of this thesis.

My family has been essential in assisting me with their love and support during my research. I wish to thank my parents, Donald and Patricia Becker for their continued love and encouragement, and my brother, Matthew Becker, for his comradeship.

Portions of my work have been supported by Lockheed Martin Corporation. I am grateful for its support.

TABLE OF CONTENTS

LIST OF TABLES

LIST OF FIGURES

Chapter I

Introduction

Asteroids and comets have been popular subjects of study recently, both for scientific and commercial reasons. These bodies may contain material remaining from the inception of the solar system, giving insights into its creation and history. It has also been speculated that initial deposits of water and other minerals on Earth came from asteroids or comets that impacted its surface. Commercially, they provide a potential source of valuable materials for mining purposes. A number of recent missions have studied asteroids or comets, including ISEE-3, Giotto, Galileo, and NEAR (which performed a flyby of the Asteroid 253 Mathilde, and is in route to its rendezvous with 433 Eros in 2000). Many more missions are currently being planned, such as the Near Earth Asteroid Prospector (NEAP), Stardust, MUSES-C, and Rosetta.

Using an analytic method to calculate suitable orbits about such small and irregularly shaped bodies can be difficult. There are a number of strong perturbing effects, which leads to a complex force model. The nonspherical shape of the body, gravitational effects from the Sun and Jupiter, and solar radiation pressure are some of the more significant perturbations. Numerical solutions would be required to properly include them. Numerical simulations can be used as a "trial and error" method to find suitable orbits. Differential corrections can sometimes provide a method of calculating periodic orbits.

Polar periodic orbits would likely be desirable for spacecraft missions for two reasons. Polar orbits would admit viewing of the entire surface of the central body. Equatorial orbits, on the other hand, do not allow viewing of the poles by the spacecraft. Periodic orbits, or orbits where the state variables return to the initial conditions after one orbit, would be desirable for their predictable nature. Differential corrections can be applied to orbits that are nearly periodic to force the state variables to be very close to the initial conditions after one revolution. Stationkeeping costs may also be very small on such orbits, leading to more available room for scientific equipment or other subsystems of the spacecraft.

Resonance, the condition where the satellite orbital period is commensurate with the rotational period of the asteroid, may also be exploited to produce orbits that do not crash or escape. Resonance usually has adverse effects in orbital mechanics, but in this study resonance orbits are found to provide good initial estimates to use in the differential corrections algorithm (described in Chapter V). In addition, the evolution of the rate of change in periapsis distance over the course of one revolution is studied for these orbits. This evolution can provide insight as to whether the orbit will crash (or escape) or if it is a usable orbit.

A. Problem Definition

This study is an investigation into polar periodic orbits about asteroids and comets. This objective has a number of requirements that must be addressed. An appropriate force model must be developed. No model can effectively include all possible perturbations that could be encountered. The objective is to choose a model that includes higher order effects to some degree, is flexible enough to allow for a variety of "real world" situations, but is also simple enough to allow computations using conventional modeling techniques. The most significant force to model is the nonspherical shape of the central body. This is done using two different techniques: elliptic integrals and a harmonic expansion. Other perturbations need to be considered as well, especially solar and Jovian gravity, and solar radiation pressure.

A combination of semi-analytic and numerical methods is used. Each approach has advantages and disadvantages. Analytic methods in general require more work "up front" from the designer, easing computer requirements (memory, processor speed, etc). Closed-form solutions may be possible, which can lead to a relatively straightforward method for finding suitable orbits. There is also little roundoff error involved, so longer periods of time can be studied. On the other hand, simplifying assumptions most likely will need to be made in order for closed-form solutions to be found, making those solutions less accurate. Numerical solutions can be more easily implemented by computer since not as much initial work is required. Fewer assumptions are necessary as well, making the simulations more accurate over a certain amount of time. Roundoff

error will degrade the solution accuracy, however, and so numerical simulations should not be trusted for long periods of time. In addition, it may be harder to determine a general method for finding solutions solely using numerical integration programs, as the simulation of a single orbit gives no indication of the stability characteristics of other orbits. Substantial amounts of computer resources may also be required, depending on the nature of the problem. This study attempts to combine analytical with numerical principles in order to gain the advantages of both. Simplifying assumptions germane to the problem are made, but several numerical simulations are used to study a variety of orbits.

To compute periodic polar orbits, a differential correction algorithm is derived for the asteroids in question, and resonance orbits will be used as inputs to this algorithm. Non-resonance orbits will also be studied to determine the effects of resonance in this model. In addition, the rate of change of periapsis distance will be calculated over the course of one orbit as a way of further studying the dynamics.

B. Previous Contributions

Orbits about asteroids and comets have been popular subjects of study recently. The proliferation of space missions to such bodies has inspired much research. From a dynamics perspective, studying these orbits provides an opportunity to model several different perturbations and compare the results to the orbits of actual spacecraft.

Studies of these orbits can be classified into three general groups: equatorial orbits (where the inclination is 0°), polar orbits (where the inclination is near or equal to 90°), and orbits of other inclinations. Several authors have studied nonspherical effects of the central body on equatorial orbits. German and Friedlander modeled the central body both as an ellipsoid and a bifurcated dumbbell [1]. They used Eros as the model for their ellipsoid and simulated a number of orbits about it, including orbits at the equilibrium points. Scheeres studied Vesta, Gaspra, Ida and Eros using a triaxial ellipsoid [2], studying their equilibrium points and zero-velocity surfaces in detail, and determining some repeating orbits using differential corrections. Retrograde orbits were also studied.

Chauvineau, Farinella, and Mignard used surface of section plots to study the general nature of equatorial orbits about triaxial ellipsoids [3].

Considering solar gravity, Chauvineau and Mignard used surface of section plots in Reference [4]. Hamilton and Burns studied the zero-velocity surfaces and equilibrium points of the Sun-asteroid-satellite system to find bound orbits [5]. They concluded that retrograde orbits appear to be more stable than prograde orbits. The Jovian gravitational effects have also been studied. Zhang and Innanen concluded that these effects can be safely ignored [6]. Chauvineau and Mignard have also studied Jovian gravity [7], as well as the effects of passes of nearby asteroids [8].

Polar orbits have not been studied as extensively, perhaps due to the fact that the equation of motion become simplified when considering equatorial orbits, if the central body is symmetric about its equator. Utashima studied solar radiation pressure, under the assumption that it is the most significant effect after the gravitational harmonics [9]. Scheeres has also studied polar orbits [10].

C. Scope of the Present Study

In this study, the central body is modeled as a triaxial ellipsoid with no other perturbations included. The model can be modified later to include other significant perturbations such as the effects of solar and Jovian gravity, more complex force models, solar radiation pressure, and the presence of nearby asteroids. A general method for calculating the orbital elements needed for periodic orbits is developed for this model. Differential correction programs are used on a series of initial conditions, with resonance orbits to be used as the initial estimates. Non-resonance orbits are also studied to determine the effects of resonance on the orbits in question. Resonance usually has adverse effects on orbits that have been studied about bodies such as the Earth and Moon. However, they are studied here to determine if resonance can "lock" the satellite into a stable orbit, preventing it from crashing or escaping. For each of these orbits, the evolution of the rate of change of periapsis distance with respect to mean anomaly was studied. The rate of change is calculated using Lagrange's Planetary Equations with the potential expressed in terms of orbital elements [11] and also expressed as an infinite

series of harmonic coefficients. This evolution is then compared to the results of the differential correction process, providing some insight into the success of the differential correction algorithm convergence.

Chapter II

Background

The problem of determining potentially useful orbits about irregularly shaped bodies is extensive and requires a large amount of background material in order to generate an accurate model. This chapter focuses on the mathematical basis for the analyses to follow. The bulk of the work in this chapter is taken from previous studies.

A. Model Definition

The problem explored in the current study is different from more classical orbit dynamics problems such as the two- and three-body problems. The two-body problem assumes two spherical masses orbit their common center of mass, with no other gravitational effects included. The restricted three-body problem assumes that the satellite is in the presence of two massive bodies (e.g., Earth and the Moon). These assumptions are appropriate when orbiting a nearly spherical, massive body such as the Earth or the Sun. When orbiting asteroids and comets, however, one can not apply these assumptions while maintaining accuracy in the resulting simulations. Asteroids are highly nonspherical. Images of several asteroids show them to be more cylindrical than spherical in shape. They are also much less massive than the planets. Vesta, one of the largest main belt asteroids, is one one-millionth as massive as the Earth. Being so small, the gravitational attractions of external bodies become much more significant. The Sun is the dominant body in the solar system, with Jupiter and other asteroids also notable due to their proximity.

The choice of model to use for simulations is critical. No model can effectively include all possible perturbations that could be encountered. No asteroid or comet will have the exact dimensions of the shape chosen here. The objective is to choose a model that includes higher order effects to some degree, is flexible enough to allow for a variety of "real world" situations, but is also simple enough to allow computations using conventional modeling techniques. The model choice should include the most significant perturbations initially, with less crucial effects to be added later. Adding higher order effects generally affect stable orbits by making them unstable. There are some special

exceptions, such as halo orbits, where higher order terms can be used to create usable orbits. If no candidate orbits can be found in the first-order model, none are likely to exist in more complex models. Assuming some possible orbits are identified initially, they will be used as starting points when searching for usable orbits when other effects have been added.

1. The Triaxial Ellipsoid

In this study, the central body is modeled as a triaxial ellipsoid with semiaxes α, β and γ. The only force considered to be acting on the satellite is the gravitational force of this central body, including nonspherical effects. All other forces (external gravity, comet outgassing, etc.) are ignored initially. A constant density of 3.5 g/cm^3 will be used, which is consistent with studies showing that most main-belt asteroids have densities between 2.5 and 3.5 g/cm^3. Additionally, the body is assumed to be rotating with a constant angular velocity about the z-axis, the axis with the largest moment of inertia. This provides the rotationally stable configuration. The orbit of the primary body about the Sun is also assumed to be unaffected by its satellite. This model admits a wide variety of shapes to approximate actual asteroids to some degree. The gravitational potential is calculated in this study using one of two methods: elliptic integrals or a harmonic series. Both can be easily calculated using standard mathematical techniques.

Figure 2-1 shows the central body, the position of the spacecraft (given by point P), and the reference frames necessary to derive the equations of motion, with their origins defined as coinciding with the center of the body. Two reference frames are necessary: an inertially fixed reference frame defined by $(\hat{x}_I, \hat{y}_I, \hat{z}_I)$, and a frame defined by $(\hat{x}, \hat{y}, \hat{z})$ that is fixed with respect to the primary body and rotating with a constant angular velocity ω with respect to the inertial frame.

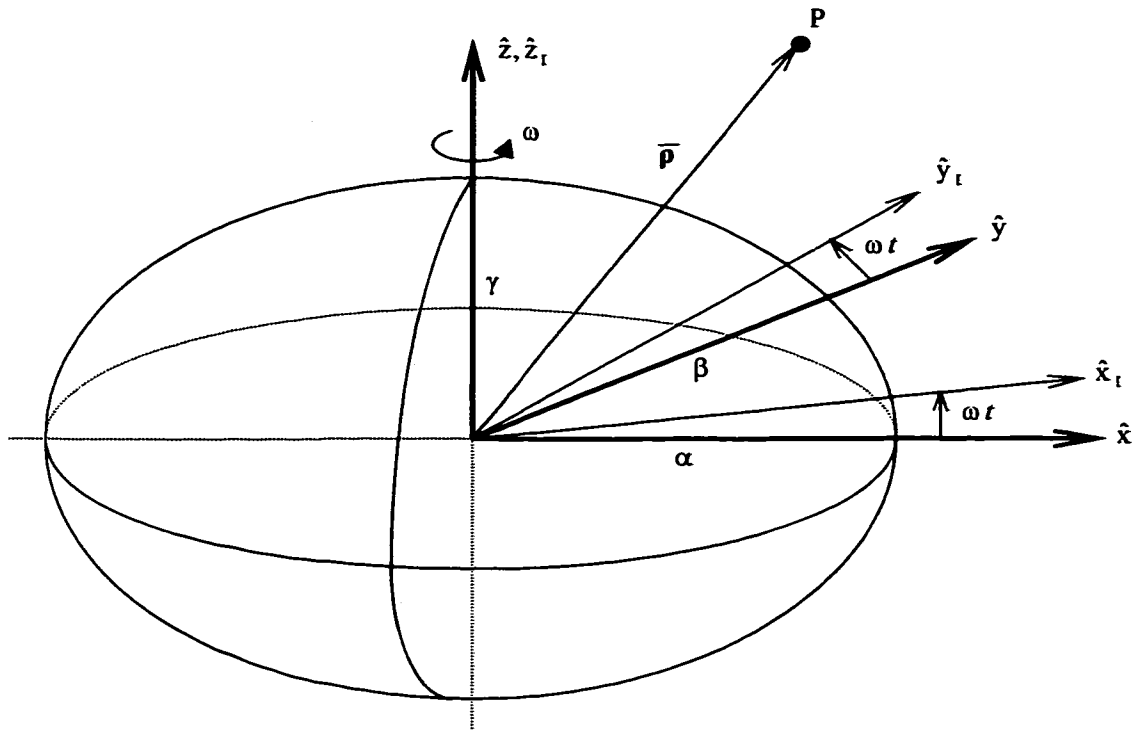

Figure 2-1. Central Body Geometry and Reference Frames

Table 2-1 shows the physical parameters used for the asteroids in this study. These values have been taken from Reference [2] in order to facilitate comparison of the results of this study with other studies.

Table 2-1. Asteroid Parameters

	Vesta	Ida	Eros	Gaspra
α (km)	265	28	20.0	9.5
β (km)	250	12	7.1*	6
γ (km)	220	10.5	7.0	5.5
Rotational period (hrs)	5.3	4.63	5.27	7
Density ρ (g/cm^3)	3.5	3.5	3.2	3.5
Gravitational parameter μ (km^3/sec^2)	14.26	3.451×10^{-3}	4.793×10^{-4}	3.067×10^{-4}
1:1 estimated resonance distance (km)	508.48	28.96	20.002	17.02
2:1 estimated resonance distance (km)	807.16	45.97	31.75	27.02
3:1 estimated resonance distance (km)	1059.89	60.24	41.61	35.41
4:1 estimated resonance distance (km)	1281.29	72.97	50.40	42.895

2. Equations of Motion

The position of the spacecraft is defined by

$$\bar{\rho} = x\hat{x} + y\hat{y} + z\hat{z} \tag{2-1}$$

The $\hat{x} - \hat{y} - \hat{z}$ frame is fixed with respect to the central body, with the origin at the geometric center of the body, and rotating about the z-axis with constant angular velocity ω. All equations of motion will be expressed in terms of this rotating frame. Since the mass of the satellite is assumed to be negligible, the rotating frame experiences no nutation or precession. A second, inertially fixed frame is also centered at the origin, but not rotating with the body. To derive the equations of motion, Newton's Second Law of Motion is used:

$$\bar{F} = m_3 {}^{I}\ddot{\bar{\rho}} \tag{2-2}$$

---

* The value of β has been modified from Scheeres' value of 7.0 to 7.1 to avoid singularities in the potential function when using elliptic integrals.

Dots represent differentiation with respect to time, and the "I" superscript denotes differentiation with respect to the inertial reference frame. Since the vector $\bar{\rho}$ is expressed in terms of the rotating frame, a conversion is needed to take derivatives with respect to the inertial frame, through the well-known kinematic equation

$$^{I}\dot{\bar{\rho}}=^{R}\dot{\bar{\rho}}+^{I}\bar{\omega}^{R}\times\bar{\rho} \tag{2-3}$$

where $^{R}\dot{\bar{\rho}}$ is the velocity of the point P with respect to the rotating reference frame, $^{I}\bar{\omega}^{R}$ is the angular velocity of the rotating frame with respect to the inertial frame, and $^{I}\bar{\omega}^{R}=\omega\hat{z}$. Taking the derivative and collecting like terms leads to

$$^{I}\dot{\bar{\rho}}=(\dot{x}-\omega y)\hat{x}+(\dot{y}+\omega x)\hat{y}+\dot{z}\hat{z} \tag{2-4}$$

Taking the derivative of (2-4) and assuming that $^{I}\bar{\omega}^{R}$ is constant in both direction and magnitude (since the body does not nutate or precess) leads to an expression for the acceleration of the particle

$$^{I}\ddot{\bar{\rho}}=^{R}\ddot{\bar{\rho}}+2^{I}\bar{\omega}^{R}\times^{R}\dot{\bar{\rho}}+^{I}\bar{\omega}^{R}\times\left(^{I}\bar{\omega}^{R}\times\bar{\rho}\right) \tag{2-5}$$

Substituting the values for each term produces

$$^{I}\ddot{\bar{\rho}}=(\ddot{x}-2\omega\dot{y}-\omega^{2}x)\hat{x}+(\ddot{y}+2\omega\dot{x}-\omega^{2}y)\hat{y}+\ddot{z}\hat{z} \tag{2-6}$$

The only force experienced by the particle is the gravitational force of the attracting mass. This force will be expressed in terms of the potential V.

$$\frac{\bar{F}}{m_3}=\frac{\partial V}{\partial x}\hat{x}+\frac{\partial V}{\partial y}\hat{y}+\frac{\partial V}{\partial z}\hat{z} \tag{2-7}$$

The resulting second order differential equations of motion will then be

$$\ddot{x}=\frac{\partial V}{\partial x}+2\omega\dot{y}+\omega^{2}x \tag{2-8a}$$

$$\ddot{y}=\frac{\partial V}{\partial y}-2\omega\dot{x}+\omega^{2}y \tag{2-8b}$$

$$\ddot{z}=\frac{\partial V}{\partial z} \tag{2-8c}$$

The potential is a function of the size, shape, and mass of the central body. For a triaxial ellipsoid, one of two functions can be used to calculate the potential and its derivatives.

i. Elliptic Integral Representation

The first expression of the potential involves elliptic integrals. The potential is given by

$$V = G\pi\rho\alpha\beta\gamma \int_{\kappa}^{\infty} \left(1 - \frac{x^2}{\alpha^2+s} - \frac{y^2}{\beta^2+s} - \frac{z^2}{\gamma^2+s}\right) \cdot \frac{ds}{\sqrt{(\alpha^2+s)(\beta^2+s)(\gamma^2+s)}} \tag{2-9}$$

where α, β, and γ are the semiaxes of the ellipsoid, x, y, and z define the position of the orbiting particle, and κ is a nondimensional quantity, defined as the largest root of the equation

$$\frac{x^2}{\alpha^2+\kappa} + \frac{y^2}{\beta^2+\kappa} + \frac{z^2}{\gamma^2+\kappa} = 1 \tag{2-10}$$

Definite integrals with an upper bound of infinity can not be calculated directly. A transformation is required, as outlined in Reference [12]. The final results for the potential and its derivatives are

$$\begin{aligned} V = \frac{2\pi\rho\alpha\beta\gamma}{\sqrt{\alpha^2-\gamma^2}} \Bigg\{ & \left[1 - \frac{x^2}{\alpha^2-\beta^2} + \frac{y^2}{\alpha^2-\beta^2}\right] F(\omega_\kappa, k) \\ & + \left[\frac{x^2}{\alpha^2-\beta^2} - \frac{(\alpha^2-\gamma^2)y^2}{(\alpha^2-\beta^2)(\beta^2-\gamma^2)} + \frac{z^2}{\beta^2-\gamma^2}\right] E(\omega_\kappa, k) \\ & + \left[\frac{\gamma^2+\kappa}{\beta^2-\gamma^2}y^2 - \frac{\beta^2+\kappa}{\beta^2-\gamma^2}z^2\right] \frac{\sqrt{\alpha^2-\gamma^2}}{\sqrt{(\alpha^2+\kappa)(\beta^2+\kappa)(\gamma^2+\kappa)}} \Bigg\} \end{aligned} \tag{2-11}$$

$$\frac{\partial V}{\partial x} = -\frac{4G\pi\alpha\beta\gamma\, x}{(\alpha^2-\beta^2)(\alpha^2-\gamma^2)^{1/2}} [F(\omega_\kappa, k) - E(\omega_\kappa, k)] \tag{2-12a}$$

$$\frac{\partial V}{\partial y} = \frac{4G\pi\rho\alpha\beta\gamma\, y}{(\alpha^2-\gamma^2)^{1/2}}\left[\frac{F(\omega_\kappa,k)}{\alpha^2-\beta^2} - \frac{(\alpha^2-\gamma^2)E(\omega_\kappa,k)}{(\alpha^2-\beta^2)(\beta^2-\gamma^2)} + \frac{(\gamma^2+\kappa)(\alpha^2-\gamma^2)^{1/2}}{(\beta^2-\gamma^2)\sqrt{(\alpha^2+\kappa)(\beta^2+\kappa)(\gamma^2+\kappa)}}\right] \tag{2-12b}$$

$$\frac{\partial V}{\partial z} = \frac{4G\pi\alpha\beta\gamma\, z}{(\alpha^2-\gamma^2)^{1/2}(\beta^2-\gamma^2)}\left[E(\omega_\kappa,k) - \frac{(\beta^2+\kappa)(\alpha^2-\gamma^2)^{1/2}}{\sqrt{(\alpha^2+\kappa)(\beta^2+\kappa)(\gamma^2+\kappa)}}\right] \tag{2-12c}$$

where $\omega_\kappa = \sin^{-1}\sqrt{\frac{\alpha^2-\gamma^2}{\alpha^2+\kappa}}$, $k = \sqrt{\frac{\alpha^2-\beta^2}{\alpha^2-\gamma^2}}$, and $F(\omega_\kappa,k)$ and $E(\omega_\kappa,k)$ are the elliptic integral functions of the first and second kind, respectively. They are computed according to the procedure outlined in Reference [13].

The second derivatives of the potential function will also be required. These derivatives are easily computed since the quantity κ can be assumed independent of x, y, and z[12]. The second derivatives are shown here.

$$V_{xx} = \frac{\partial^2 V}{\partial x^2} = -\frac{4G\pi\alpha\beta\gamma}{(\alpha^2-\beta^2)(\alpha^2-\gamma^2)^{1/2}}[F(\omega_\kappa,k) - E(\omega_\kappa,k)] \tag{2-13a}$$

$$V_{yy} = \frac{\partial^2 V}{\partial y^2} = \frac{4G\pi\rho\alpha\beta\gamma}{(\alpha^2-\gamma^2)^{1/2}}\left[\frac{F(\omega_\kappa,k)}{\alpha^2-\beta^2} - \frac{(\alpha^2-\gamma^2)E(\omega_\kappa,k)}{(\alpha^2-\beta^2)(\beta^2-\gamma^2)} + \frac{(\gamma^2+\kappa)(\alpha^2-\gamma^2)^{1/2}}{(\beta^2-\gamma^2)\sqrt{(\alpha^2+\kappa)(\beta^2+\kappa)(\gamma^2+\kappa)}}\right] \tag{2-13b}$$

$$V_{zz} = \frac{\partial^2 V}{\partial z^2} = \frac{4G\pi\alpha\beta\gamma}{(\alpha^2-\gamma^2)^{1/2}(\beta^2-\gamma^2)}\left[E(\omega_\kappa,k) - \frac{(\beta^2+\kappa)(\alpha^2-\gamma^2)^{1/2}}{\sqrt{(\alpha^2+\kappa)(\beta^2+\kappa)(\gamma^2+\kappa)}}\right] \tag{2-13c}$$

ii. Harmonic Series Expansion

The potential can also be expressed in terms of a harmonic series expansion. In this method, the potential is expressed in terms of spherical coordinates r, L, and λ as

$$V = \frac{\mu}{r}\left[1 + \sum_{n=2}^{\infty}\sum_{m=0}^{n}\left(\frac{\alpha}{r}\right)^{n} \cdot P_{nm}(\sin L)(C_{nm}\cos m\lambda + S_{nm}\sin m\lambda)\right] \quad (2\text{-}14)$$

where μ is the gravitational coefficient of the central body (equal to product of the Universal Gravitational Constant and the mass), and r, L, and λ are the spherical coordinates defining the position of the orbiting particle (r is the radius from the center of the body, L is the "latitude" and λ the "longitude" of the particle). P_{nm} is the associated Legendre polynomial of order "n" and degree "m", and C_{nm} and S_{nm} are nondimensional quantities defining the shape of the central body. In general, as n and m increase, the corresponding C_{nm} and S_{nm} values decrease (approach zero). When orbiting an oddly shaped body, these values must be determined from precise measurements taken over many orbits. For the ellipsoidal model used in this study, however, these coefficients can be calculated numerically using inertia integrals. Table 2-2 shows the first few terms for the asteroids used in this study. Note that, since this shape is symmetric about each axis, $C_{nm} = 0$ for all odd n,m and $S_{nm} = 0$ for all n,m.

Table 2-2. Asteroid Harmonic Shape Coefficients

		Vesta	Ida	Gaspra
n	**m**	C_{nm}	C_{nm}	C_{nm}
2	0	-1.02314×10^{-1}	-1.80485×10^{-1}	-1.45706×10^{-1}
2	2	5.50018×10^{-3}	4.08163×10^{-2}	3.00554×10^{-2}
4	0	1.14752×10^{-2}	4.91813×10^{-2}	3.04896×10^{-2}
4	2	-2.00980×10^{-4}	-2.63097×10^{-3}	-1.56402×10^{-3}
4	4	5.40214×10^{-6}	2.97495×10^{-4}	1.61308×10^{-4}
6	0	-1.70435×10^{-3}	-1.94875×10^{-2}	-9.30400×10^{-3}
6	2	1.73341×10^{-5}	4.76660×10^{-4}	2.22228×10^{-4}
6	4	-1.53532×10^{-7}	-1.49148×10^{-5}	-6.52880×10^{-6}
6	6	2.75118×10^{-9}	1.12432×10^{-6}	4.48906×10^{-7}

3. Nondimensionalization of Equations of Motion

The equations of motion are most useful in the differential correction process when expressed in nondimensional form. In this form, one "distance unit" is defined to be the largest semiaxis of the asteroid, and one "time unit" is given $1/\omega$, i.e., the inverse of the rotational rate of the asteroid.

4. Equilibrium Points

Equilibrium points are those points where the sum of the forces in the rotating frame is zero. They are found by setting the velocity and acceleration components in the equations of motion equal to zero and then calculating the corresponding values for the position. When modeling the potential using an ellipsoidal shape, four equilibrium points are found[1], [2], all of which are in the equatorial plane of the asteroid. Two equilibrium points are located on the x-axis and two on the y-axis of the rotating reference frame. These points are found by applying the Newton-Raphson method for finding zeros to the equations of motion. Table 2-3 shows the equilibrium points for the asteroids considered in this study. A mass located at any of these points will theoretically remain there forever, since there is no net force acting on it. When numerically integrating, however, numerical "noise" is invariably incurred, resulting in the mass moving away from the equilibrium point. Equilibrium solutions are important for several reasons. As a practical application, a satellite located at an equilibrium point will "stare" at the body at the same orientation for a long period of time (although small maneuvers may be necessary to keep the satellite at the desired location, and the polar regions will not be in view). In addition, equilibrium points can give insight to the stability of orbits about the asteroid, since the equilibrium points themselves can be classified as either "stable" or "unstable." They can also be used to verify the correctness of the numerical integration algorithm. If a mass placed at such a point moves away from it immediately, it can be an indication that the numerical integrator and/or the equations of motion are faulty.

Table 2-3. Asteroid Equilibrium Points

Asteroid	x_{eq} (km)	y_{eq} (km)
Gaspra	±17.71	±16.75
Ida	±33.89	±27.21
Eros	±23.91	±18.64
Vesta	±514.36	±509.80

As an example, consider Figure 2-2. This figure show results of simulations of masses placed at the major and minor axis points of Ida, with the distance "r" from the center of the asteroid plotted as a function of time. The mass at the major axis point

remains there roughly twelve hours before moving rapidly away from the equilibrium point. The mass at the minor axis, however, stays at the same point roughly thirty hours before moving away. Both points appear to be unstable. A rigorous mathematical study of the stability of these points has been completed[2], but is not presented here.

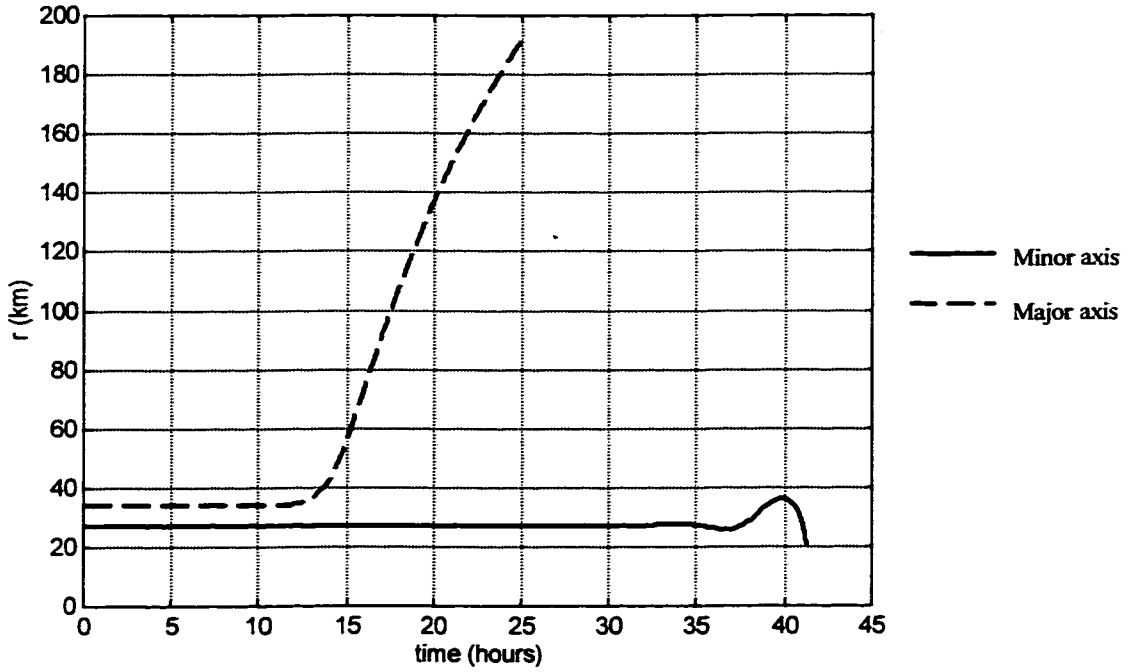

Figure 2-2. Ida Equilibrium Point Orbits

5. Inclusion of Solar Gravity

When including solar gravity in the force model, a new set of reference frames must be defined. The inertial frame for the system will now be at the center of the Sun, instead of the asteroid. The rotating frame in terms of which the equations of motion will be expressed (designated the "asteroid frame") will still be rotating with the asteroid, with its origin at the center of the body. A third, intermediate rotating frame is also necessary to express the rotation of the asteroid about the Sun. These frames are depicted in Figure 2-3.

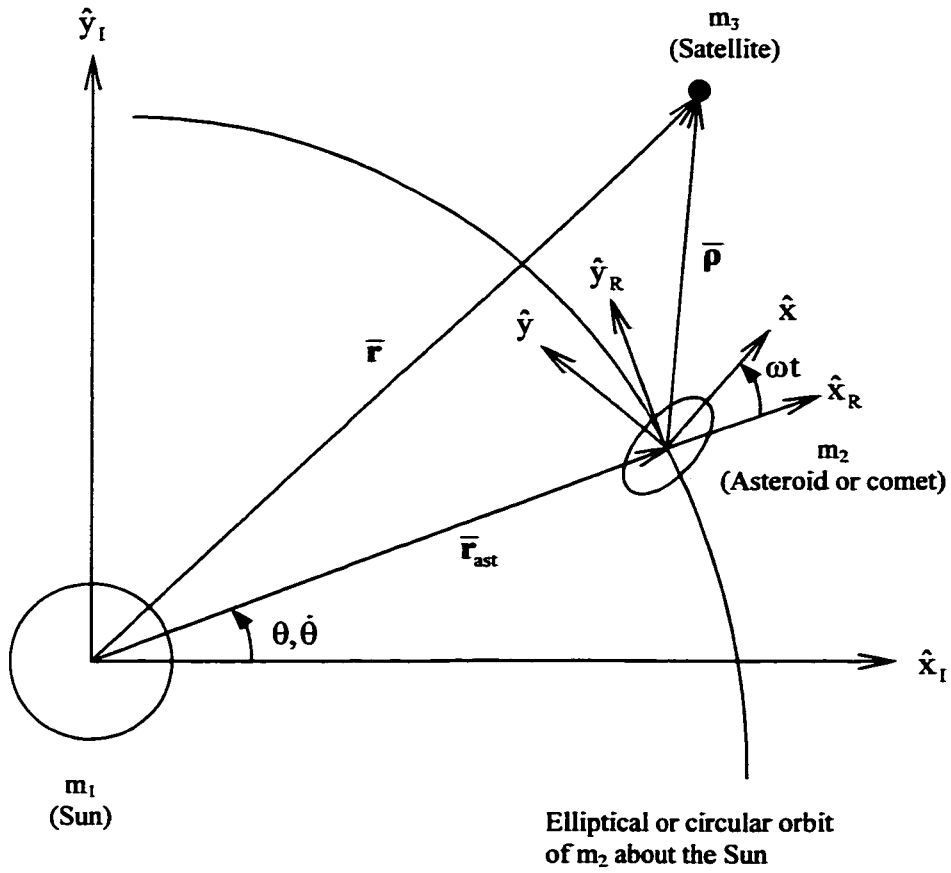

Figure 2-3. Sun-Asteroid-Satellite Model Reference Frames

For this model, Newton's Second Law takes the form

$$\bar{F} = m\,{}^I\ddot{\bar{r}} \tag{2-15}$$

The vector $\bar{r}$ is the sum of the vectors defining the position of the asteroid with respect to the sun and the satellite with respect to the asteroid, i.e.,

$$\bar{r} = \bar{r}_{ast} + \bar{\rho} \tag{2-16}$$

Taking the derivative, using (2-3) leads to

$${}^I\dot{\bar{r}} = {}^{R'}\dot{\bar{r}}_{ast} + {}^I\bar{\omega}^{R'} \times \bar{r}_{ast} + {}^{R'}\dot{\bar{\rho}} + {}^I\bar{\omega}^{R'} \times \bar{\rho} \tag{2-17}$$

which is tenable as long as the vector $\bar{r}_{ast}$ is expressed in terms of the asteroid frame.

Taking the derivative again produces

$${}^I\ddot{\bar{r}} = \ddot{\bar{\rho}} + 2\,{}^I\bar{\omega}^{R'} \times \dot{\bar{\rho}} + {}^I\bar{\omega}^{R'} \times \left({}^I\bar{\omega}^{R'} \times \bar{\rho}\right) + \ddot{\bar{r}}_{ast} + 2\,{}^I\bar{\omega}^{R'} \times \dot{\bar{r}}_{ast} + {}^I\bar{\omega}^{R'} \times \left({}^I\bar{\omega}^{R'} \times \bar{r}_{ast}\right) \tag{2-18}$$

Note that the R' superscript has been removed from the derivative terms for sake of brevity. All derivatives are with respect to the asteroid frame unless otherwise noted. In addition, ${}^{I}\dot{\bar{\omega}}^{R'} = 0$ since the asteroid does not nutate or precess, and similarly for its orbit about the Sun.

With (2-18) derived, the task remains to determine the expressions for each term. The vector defining the direction from the Sun to the asteroid is given by $\bar{r}_{ast} = r_{ast}\hat{x}_R$. Using direction cosine matrices, this vector is expressed in terms of the asteroid frame by

$$\bar{r}_{ast} = r_{ast}\cos(\theta - \omega t)\hat{x} + r_{ast}\sin(\theta - \omega t)\hat{y} \tag{2-19}$$

Taking the derivative with respect to time and the asteroid frame gives

$$\begin{aligned} {}^{R'}\dot{\bar{r}}_{ast} = &\left[\dot{r}_{ast}\cos(\theta - \omega t) - r_{ast}(\dot{\theta} - \omega)\sin(\theta - \omega t)\right]\hat{x} + \\ &\left[\dot{r}_{ast}\sin(\theta - \omega t) + r_{ast}(\dot{\theta} - \omega)\cos(\theta - \omega t)\right]\hat{y} \end{aligned} \tag{2-20}$$

Define $\varepsilon = \theta - \omega t$, so $\dot{\varepsilon} = \dot{\theta} - \omega$. Then

$${}^{R'}\dot{\bar{r}}_{ast} = \left[\dot{r}_{ast}\cos\varepsilon - r_{ast}\dot{\varepsilon}\sin\varepsilon\right]\hat{x} + \left[\dot{r}_{ast}\sin\varepsilon + r_{ast}\dot{\varepsilon}\cos\varepsilon\right]\hat{y} \tag{2-21}$$

and

$$\begin{aligned} {}^{R'}\ddot{\bar{r}}_{ast} = &\left[\ddot{r}_{ast}\cos\varepsilon - 2\dot{r}_{ast}\dot{\varepsilon}\sin\varepsilon - r_{ast}\ddot{\theta}\sin\varepsilon - r_{ast}\dot{\varepsilon}^2\cos\varepsilon\right]\hat{x} + \\ &\left[\ddot{r}_{ast}\sin\varepsilon + 2\dot{r}_{ast}\dot{\varepsilon}\cos\varepsilon - r_{ast}\ddot{\theta}\cos\varepsilon - r_{ast}\dot{\varepsilon}^2\sin\varepsilon\right]\hat{y} \end{aligned} \tag{2-22}$$

Substituting into (2-18) and carrying through the algebra gives the acceleration of the satellite with respect to the inertial reference frame

$$\begin{aligned} {}^{I}\ddot{\bar{r}} = &\left[\ddot{x} - 2\omega\dot{y} - \omega^2 x + \ddot{r}_{ast}\cos\varepsilon - 2\dot{r}_{ast}\dot{\varepsilon}\sin\varepsilon - r_{ast}\ddot{\theta}\sin\varepsilon - r_{ast}\dot{\varepsilon}^2\cos\varepsilon - 2\omega\dot{r}_{ast}\sin\varepsilon - \right. \\ &\left. 2\omega r_{ast}\dot{\varepsilon}\cos\varepsilon - \omega^2 r_{ast}\cos\varepsilon\right]\hat{x} + \\ &\left[\ddot{y} + 2\omega\dot{x} - \omega^2 y + \ddot{r}_{ast}\sin\varepsilon - 2\dot{r}_{ast}\dot{\varepsilon}\cos\varepsilon - r_{ast}\ddot{\theta}\cos\varepsilon - r_{ast}\dot{\varepsilon}^2\sin\varepsilon + 2\omega\dot{r}_{ast}\cos\varepsilon - \right. \\ &\left. 2\omega r_{ast}\dot{\varepsilon}\sin\varepsilon - \omega^2 r_{ast}\sin\varepsilon\right]\hat{y} + \ddot{z}\hat{z} \end{aligned} \tag{2-23}$$

There are two forces acting on the point mass: the gravitational attraction from the Sun and that from the asteroid. This is expressed as

$$\bar{F} = \bar{F}_{m_1 m_3} + \bar{F}_{m_2 m_3} \tag{2-24}$$

where $\bar{F}_{m_1 m_3}$ is the gravitational force from the Sun, and $\bar{F}_{m_2 m_3}$ is the force from the asteroid. The gravitational force of the Sun can be expressed as

$$\bar{F}_{m_1 m_3} = -\frac{Gm_1 m_3}{r^3}\bar{r} = -\frac{Gm_1 m_3}{r^3}\bar{r}_{ast} - \frac{Gm_1 m_3}{r^3}\bar{\rho} \tag{2-25}$$

where $r = \left[(r_{ast}\cos\varepsilon + x)^2 + (r_{ast}\sin\varepsilon + y)^2 + z^2\right]^{1/2}$ is the distance of the satellite from the Sun. Substituting (2-1) and (2-19) into (2-25), and dividing through by m_3 leads to

$$\frac{\bar{F}_{m_1 m_3}}{m_3} = -\frac{Gm_1}{r^3}\left[r_{ast}\cos\varepsilon + x\right]\hat{x} - \frac{Gm_1}{r^3}\left[r_{ast}\sin\varepsilon + y\right]\hat{y} - \frac{Gm_1}{r^3}z\hat{z} \tag{2-26}$$

The force due to the asteroid can be expressed as in (2-7). Finally, (2-7), (2-23), and (2-26) can be substituted into (2-15) to produce the equations of motion when including solar gravity

$$\ddot{x} = \frac{1}{m_3}\frac{\partial V}{\partial x} - \frac{Gm_1}{r^3}\left[r_{ast}\cos\varepsilon + x\right] + 2\omega\dot{y} + \omega^2 x - \ddot{r}_{ast}\cos\varepsilon + 2\dot{r}_{ast}\dot{\varepsilon}\sin\varepsilon + r_{ast}\ddot{\theta}\sin\varepsilon \tag{2-27a}$$
$$+ r_{ast}\dot{\varepsilon}^2\cos\varepsilon + 2\omega\dot{r}_{ast}\sin\varepsilon + 2\omega r_{ast}\dot{\varepsilon}\cos\varepsilon + \omega^2 r_{ast}\cos\varepsilon$$

$$\ddot{y} = \frac{1}{m_3}\frac{\partial V}{\partial y} - \frac{Gm_1}{r^3}\left[r_{ast}\sin\varepsilon + y\right] - 2\omega\dot{x} + \omega^2 y - \ddot{r}_{ast}\sin\varepsilon - 2\dot{r}_{ast}\dot{\varepsilon}\cos\varepsilon + r_{ast}\ddot{\theta}\cos\varepsilon \tag{2-27b}$$
$$+ r_{ast}\dot{\varepsilon}^2\sin\varepsilon - 2\omega\dot{r}_{ast}\cos\varepsilon + 2\omega r_{ast}\dot{\varepsilon}\sin\varepsilon + \omega^2 r_{ast}\sin\varepsilon$$

$$\ddot{z} = \frac{1}{m_3}\frac{\partial V}{\partial z} - \frac{Gm_1}{r^3}z \tag{2-27c}$$

6. Derivation of Harmonic Coefficients

The harmonic coefficients are functions of the inertial integrals I_{pqr}, which are defined by Reference [1] as

$$I_{pqr} = \rho\iiint_B x^p y^q z^r dV \tag{2-28}$$

or

$$I_{pqr} = \rho\int_{-z_o}^{z_o}\int_{-y_o}^{y_o}\int_{-\alpha}^{\alpha} x^p y^q z^r dx\cdot dy\cdot dz \tag{2-29}$$

where

$$y_o = \beta\left[1 - \left(\frac{x}{\alpha}\right)^2\right]^{1/2} \tag{2-30}$$

$$z_o = \gamma\left[1-\left(\frac{x}{\alpha}\right)^2-\left(\frac{y}{\beta}\right)^2\right]^{1/2} \tag{2-31}$$

Performing the integration over z leads to

$$I_{pqr} = \frac{8\rho\gamma^{r+1}}{r+1}\int_0^{\alpha} x^p \left\{\int_0^{y_o} y^q\left[1-\left(\frac{x}{\alpha}\right)^2-\left(\frac{y}{\beta}\right)^2\right]^{\frac{r+1}{2}} dy\right\} dx \tag{2-32}$$

The integration over y, contained in the braces, is first simplified. A change of variables is required, such that $u = y/b$, $du = (1/b)\,dy$, and $u_o = y_o/b$. Then

$$\int_0^{y_o} y^q\left[1-\left(\frac{x}{\alpha}\right)^2-\left(\frac{y}{\beta}\right)^2\right]^{\frac{r+1}{2}} dy = b^{q+1}\int_0^{y_o}\left(\frac{y}{b}\right)^q\left[1-\left(\frac{x}{\alpha}\right)^2-\left(\frac{y}{\beta}\right)^2\right]^{\frac{r+1}{2}}\frac{1}{b}dy \tag{2-33}$$

Introduce another change of variables with $\varepsilon^2 = 1-(x/a)^2$, $\theta = \sin^{-1}(u/\varepsilon)$, $du = \varepsilon\cos\theta\, d\theta$ and $\theta_o = \sin^{-1}(u_o/\varepsilon)$. We can also assume that p, q, and r are all even, since $I_{pqr} = 0$ if p, q, or r is odd. Then the integral simplifies to

$$\int_0^{y_o} y^q\left[1-\left(\frac{x}{\alpha}\right)^2-\left(\frac{y}{\beta}\right)^2\right]^{\frac{r+1}{2}} dy = b^{q+1}\varepsilon^{q+r+2}\int_0^{\theta_o}\sin^q\theta\cos^{r+2}\theta\cdot d\theta \tag{2-34}$$

where

$$\theta_o = \sin^{-1}\frac{u_o}{\varepsilon} = \sin^{-1}\frac{\left[1-(x/\alpha)^2\right]^{1/2}}{\left[1-(x/\alpha)^2\right]^{1/2}} = \sin^{-1}1 = \frac{\pi}{2} \tag{2-35}$$

Therefore,

$$\int_0^{y_o} y^q\left[1-\left(\frac{x}{\alpha}\right)^2-\left(\frac{y}{\beta}\right)^2\right]^{\frac{r+1}{2}} dy = b^{q+1}\left[1-\left(\frac{x}{\alpha}\right)^2\right]^{\frac{q+r+2}{2}}\int_0^{\pi/2}\sin^q\theta\cos^{r+2}\theta\cdot d\theta \tag{2-36}$$

Using an infinite series relationship, it can be shown that

$$\int_0^{\pi/2}\sin^n u\cos^m u\, du = \frac{(n-1)(n-3)\cdots(1)(m-1)(m-3)\cdots(1)}{(n+m)(n+m-2)\cdots(2)}\frac{\pi}{2} \tag{2-37}$$

$$\int_0^{\pi/2} \cos^m u \, du = \frac{(m-1)(m-3)\cdots(1)}{(m)(m-2)\cdots(2)} \frac{\pi}{2} \tag{2-38}$$

Define a function K(n,m) such that

$$K(n,m) = \begin{cases} \dfrac{[n-1][m-1]}{[n+m]} & \text{if } n > 0 \\ \dfrac{[m-1]}{[m]} & \text{if } n = 0 \end{cases} \tag{2-39}$$

where

$$[n-1] = (n-1)(n-3)(n-5)\cdots(1) \tag{2-40}$$

$$[m-1] = (m-1)(m-3)(m-5)\cdots(1) \tag{2-41}$$

$$[m] = (m-2)(m-4)(m-6)\cdots(2) \tag{2-42}$$

Therefore

$$\int_0^{\pi/2} \sin^n u \cos^m u \, du = K(n,m)\frac{\pi}{2} \tag{2-43}$$

$$\int_0^{y_o} y^q \left[1 - \left(\frac{x}{\alpha}\right)^2 - \left(\frac{y}{\beta}\right)^2\right]^{\frac{r+1}{2}} dy = b^{q+1}\left[1 - \left(\frac{x}{\alpha}\right)^2\right]^{\frac{q+r+2}{2}} K(q, r+2)\cdot\frac{\pi}{2} \tag{2-44}$$

Substituting Equation (2-44) into Equation (2-32) and simplifying leads to

$$I_{pqr} = \frac{8\rho\beta^{q+1}\gamma^{r+1}}{r+1} K(q, r+2)\cdot\frac{\pi}{2}\cdot\int_0^{\alpha} x^p\left[1 - \left(\frac{x}{\alpha}\right)^2\right]^{\frac{q+r+2}{2}} dx \tag{2-45}$$

Since q and r are even, (q+r+2)/2 will always be a positive integer, so the integrand will be a simple polynomial expansion, which can be expanded using the Binomial Theorem.

$$\left[1 - \left(\frac{x}{\alpha}\right)^2\right]^{\frac{q+r+2}{2}} = \sum_{n=0}^{\frac{q+r+2}{2}} \binom{\frac{q+r+2}{2}}{n} (-1)^n \frac{x^{2n}}{a^{2n}} \tag{2-46}$$

$$\int_0^{\alpha} x^p \left[1-\left(\frac{x}{\alpha}\right)^2\right]^{\frac{q+r+2}{2}} dx = \alpha^{p+1} \sum_{n=0}^{\frac{q+r+2}{2}} (-1)^n \frac{1}{2n+p+1} \binom{\frac{q+r+2}{2}}{n} \tag{2-47}$$

$$I_{pqr} = \frac{8\rho\alpha^{p+1}\beta^{q+1}\gamma^{r+1}}{r+1} K(q,r+2) \cdot \frac{\pi}{2} \cdot \sum_{n=0}^{\frac{q+r+2}{2}} (-1)^n \frac{1}{2n+p+1} \binom{\frac{q+r+2}{2}}{n} \tag{2-48}$$

Finally, substitute $\rho = 3M / (4\,\pi\,\alpha\beta\gamma)$ (where M is the total mass of the asteroid) into (2-48) to obtain

$$I_{pqr} = \frac{3M}{r+1} \alpha^p \beta^q \gamma^r K(q,r+2) \sum_{n=0}^{\frac{q+r+2}{2}} (-1)^n \frac{1}{2n+p+1} \binom{\frac{q+r+2}{2}}{n} \tag{2-49}$$

7. Definition of Altitude

In this study, altitude is defined as the closest distance between the satellite and the asteroid. This quantity is defined differently than the altitude of a satellite orbiting a nearly spherical body such as the Earth, which is simply given by the difference between the distance of the satellite from the center of the body and the mean radius of the body. When orbiting a highly nonspherical body as in this study, the mean radius does not give an accurate indication of the distance from the surface. Here the altitude must be calculated using an iterative method as outlined below.

The position of the satellite is assumed to be at a point P_1, given by the coordinates (x_1, y_1, z_1). The point on the surface closest to the satellite is called P_0, given by (x_0, y_0, z_0). The point P_0 is also the point on the surface where the gradient vector $\bar{g}$ (which defines the normal vector to the surface) passes through the satellite at P_1. Using vector addition, the position of the satellite can be expressed relative to P_0 as:

$$\bar{P}_1 = \bar{P}_0 + d\,\bar{g} \tag{2-50}$$

The altitude "h" would then be the magnitude of the vector difference $\bar{P}_1 - \bar{P}_0$, i.e.,

$$h = d\,\|\bar{g}\| = d\,g \tag{2-51}$$

The point P_0 is defined by the equation of an ellipsoid:

$$\frac{x_o^2}{\alpha^2}+\frac{y_o^2}{\beta^2}+\frac{z_o^2}{\gamma^2}=1 \tag{2-52}$$

(where α, β, and γ are the semiaxes for the asteroid) or, equivalently by the function $f(x_o,y_o,z_o)$ as

$$f(x_o,y_o,z_o)=\frac{x_o^2}{\alpha^2}+\frac{y_o^2}{\beta^2}+\frac{z_o^2}{\gamma^2}-1=0 \tag{2-53}$$

and the gradient $\bar{g}$ would be defined as

$$\bar{g}=\nabla f=\frac{\partial f}{\partial x}\hat{x}+\frac{\partial f}{\partial y}\hat{y}+\frac{\partial f}{\partial z}\hat{z}=\frac{2x_o}{\alpha^2}\hat{x}+\frac{2y_o}{\beta^2}\hat{y}+\frac{2z_o}{\gamma^2} \tag{2-54}$$

Equation (2-50) is a vector equation, which can be separated into three scalar equations:

$$x_o+\frac{2x_o d}{\alpha^2}=x_l \tag{2-55}$$

$$y_o+\frac{2y_o d}{\beta^2}=y_l \tag{2-56}$$

$$z_o+\frac{2z_o d}{\gamma^2}=z_l \tag{2-57}$$

Solving Equations (2-55), (2-56) and (2-57) for x_o, y_o and z_o, respectively, and substituting the results into (2-53) leads to the final formulation for $f(x_o,y_o,z_o)$ as

$$f(x_o,y_o,z_o)=\frac{x_l^2\alpha^2}{(\alpha^2+2d)^2}+\frac{y_o^2\beta^2}{(\beta^2+2d)^2}+\frac{z_o^2\gamma^2}{(\gamma^2+2d)^2}-1=0 \tag{2-58}$$

In this equation, the known quantities are the semiaxes of the ellipsoid α, β, and γ, and the position components of the satellite x_l, y_l, and z_l. What remains is the quantity "d," which is calculated by applying a Newton-Raphson method to Equation (2-58). The position of P_0 is then calculated using Eqs. (2-55), (2-56) and (2-57), the gradient vector $\bar{g}$ calculated using Equation (2-54), and finally the altitude using Equation (2-51).

B. Lagrange's Planetary Equations

1. Definition

Lagrange's Planetary Equations provide an alternative formulation for the equations of motion for the system.

$$\frac{da}{dt} = \frac{2}{na}\frac{\partial R}{\partial M} \tag{2-59a}$$

$$\frac{de}{dt} = \frac{1-e^2}{na^2 e}\frac{\partial R}{\partial M} - \frac{\left(1-e^2\right)^{1/2}}{na^2 e}\frac{\partial R}{\partial e} \tag{2-59b}$$

$$\frac{d\omega}{dt} = -\frac{\cos i}{na^2\left(1-e^2\right)^{1/2}\sin i}\frac{\partial R}{\partial i} + \frac{\left(1-e^2\right)^{1/2}}{na^2 e}\frac{\partial R}{\partial e} \tag{2-59c}$$

$$\frac{di}{dt} = \frac{\cos i}{na^2\left(1-e^2\right)^{1/2}\sin i}\frac{\partial R}{\partial \omega} - \frac{1}{na^2\left(1-e^2\right)^{1/2}\sin i}\frac{\partial R}{\partial \Omega} \tag{2-59d}$$

$$\frac{d\Omega}{dt} = \frac{1}{na^2\left(1-e^2\right)^{1/2}\sin i}\frac{\partial R}{\partial i} \tag{2-59e}$$

$$\frac{dM}{dt} = n - \frac{1-e^2}{na^2 e}\frac{\partial R}{\partial e} - \frac{2}{na}\frac{\partial R}{\partial a} \tag{2-59f}$$

Here, R is the "disturbing function," which is simply the difference between the potential formulation and that of a perfect sphere, i.e.,

$$R = V - \frac{\mu}{r} \tag{2-60}$$

These equations use the orbital elements as the coordinate system instead of Cartesian coordinates. This makes the planetary equations quite useful, in that they directly quantify the rates of change of the orbital elements. From a mission design standpoint, knowing the changes in orbital elements instead of other coordinates gives a clearer picture of the motion of the satellite with respect to the asteroid.

2. Disturbing Function in Terms of Orbital Elements

To be useful in Equations (2-59), the disturbing function needs to be expressed in terms of the orbital elements so that the partial derivatives may be evaluated. The

formulations for the potential shown previously are in terms of Cartesian or spherical coordinates. The conversion of the disturbing function to orbital elements, which is quite complicated and not presented here, is shown in Reference [11]. The result is

$$R = \mu \sum_{\ell=2}^{\infty} \sum_{m=0}^{\ell} \left(\frac{\alpha^{\ell}}{a^{\ell+1}} \right) \sum_{p=0}^{\ell} F_{\ell mp}(i) \sum_{q=-\infty}^{\infty} G_{\ell pq}(e) \cdot S_{\ell mpq}(\omega, M, \Omega, \theta) \tag{2-61}$$

where

$$F_{\ell mp}(i) = \sum_{t}^{\min(p,k)} \frac{(2\ell - 2t)!}{t!(\ell - t)!(\ell - m - 2t)!\, 2^{2\ell - 2t}} \sin^{\ell - m - 2t} i \tag{2-62}$$

$$\times \sum_{s=0}^{m} \binom{m}{s} \cos^{s} i \sum_{c=0}^{p-t} \binom{\ell - m - 2t + s}{c} \binom{m - s}{p - t - c} (-1)^{c-k}$$

$$G_{\ell pq}(e) = (-1)^{|q|} (1 + \beta^2)^{\ell} \beta^{|q|} \sum_{k=0}^{\infty} P_{\ell pqk} Q_{\ell pqk} \beta^{2k} \tag{2-63}$$

$$\beta = \frac{e}{1 + \sqrt{1 - e^2}} \tag{2-64}$$

$$P_{\ell pqk} = \sum_{r=0}^{h} \binom{2p' - 2\ell}{h - r} \frac{(-1)^r}{r!} \left(\frac{(\ell - 2p' + q')e}{2\beta} \right)^r \tag{2-65a}$$

$$h = \begin{cases} k + q' & \text{if} \quad q' \geq 0 \\ k & \text{if} \quad q' < 0 \end{cases} \tag{2-65b}$$

$$Q_{\ell pqk} = \sum_{r=0}^{h} \binom{-2p'}{h - r} \frac{1}{r!} \left(\frac{(\ell - 2p' + q')e}{2\beta} \right)^r \tag{2-66a}$$

$$h = \begin{cases} k & \text{if} \quad q' \geq 0 \\ k - q' & \text{if} \quad q' < 0 \end{cases} \tag{2-66b}$$

$$p' = \begin{cases} \ell - p & \text{if} \quad p > \ell/2 \\ p & \text{if} \quad p \leq \ell/2 \end{cases} \tag{2-66c}$$

$$q' = \begin{cases} -q & \text{if} \quad p > \ell/2 \\ q & \text{if} \quad p \leq \ell/2 \end{cases} \tag{2-66d}$$

$$S_{\ell mpq}(\omega,M,\Omega,\theta)=\begin{bmatrix} C_{\ell m} \\ -S_{\ell m} \end{bmatrix}_{\ell-m\ \text{odd}}^{\ell-m\ \text{even}} \cos[(\ell-2p)\omega+(\ell-2p+q)M+m(\Omega-\theta)] \tag{2-67}$$

$$+\begin{bmatrix} S_{\ell m} \\ C_{\ell m} \end{bmatrix}_{\ell-m\ \text{odd}}^{\ell-m\ \text{even}} \sin[(\ell-2p)\omega+(\ell-2p+q)M+m(\Omega-\theta)]$$

For the model in this study, $C_{lm}=0$ for l or m odd, and $S_{lm}=0$ for all l and m. Therefore (2-67) can be simplified to

$$S_{\ell mpq}(\omega,M,\Omega,\theta)=C_{\ell m}\cos[(\ell-2p)\omega+(\ell-2p+q)M+m(\Omega-\theta)] \tag{2-68}$$

Taking derivatives of this disturbing function is simplified by the fact that each term in (2-61) is a function of only one of the orbital elements (except for the function S). The infinite summation over "q", however, adds significant computational time. In addition, the infinite summation over "k" in (2-63) is also expensive to compute.

The derivatives are shown here

$$\frac{\partial R}{\partial a}=-\mu\sum_{\ell=2}^{\infty}\sum_{m=0}^{\ell}(\ell+1)\left(\frac{\alpha^{\ell}}{a^{\ell+2}}\right)\sum_{p=0}^{\ell}F_{\ell mp}(i)\sum_{q=-\infty}^{\infty}G_{\ell pq}(e)\cdot S_{\ell mpq}(\omega,M,\Omega,\theta) \tag{2-69a}$$

$$\frac{\partial R}{\partial e}=\mu\sum_{\ell=2}^{\infty}\sum_{m=0}^{\ell}\left(\frac{\alpha^{\ell}}{a^{\ell+1}}\right)\sum_{p=0}^{\ell}F_{\ell mp}(i)\sum_{q=-\infty}^{\infty}\frac{\partial G_{\ell pq}(e)}{\partial e}\cdot S_{\ell mpq}(\omega,M,\Omega,\theta) \tag{2-69b}$$

$$\frac{\partial R}{\partial i}=\mu\sum_{\ell=2}^{\infty}\sum_{m=0}^{\ell}\left(\frac{\alpha^{\ell}}{a^{\ell+1}}\right)\sum_{p=0}^{\ell}\frac{\partial F_{\ell mp}(i)}{\partial i}\sum_{q=-\infty}^{\infty}G_{\ell pq}(e)\cdot S_{\ell mpq}(\omega,M,\Omega,\theta) \tag{2-69c}$$

$$\frac{\partial R}{\partial \omega}=\mu\sum_{\ell=2}^{\infty}\sum_{m=0}^{\ell}\left(\frac{\alpha^{\ell}}{a^{\ell+1}}\right)\sum_{p=0}^{\ell}F_{\ell mp}(i)\sum_{q=-\infty}^{\infty}G_{\ell pq}(e)\cdot\frac{\partial S_{\ell mpq}(\omega,M,\Omega,\theta)}{\partial \omega} \tag{2-69d}$$

$$\frac{\partial R}{\partial \Omega}=\mu\sum_{\ell=2}^{\infty}\sum_{m=0}^{\ell}\left(\frac{\alpha^{\ell}}{a^{\ell+1}}\right)\sum_{p=0}^{\ell}F_{\ell mp}(i)\sum_{q=-\infty}^{\infty}G_{\ell pq}(e)\cdot\frac{\partial S_{\ell mpq}(\omega,M,\Omega,\theta)}{\partial \Omega} \tag{2-69e}$$

$$\frac{\partial R}{\partial M}=\mu\sum_{\ell=2}^{\infty}\sum_{m=0}^{\ell}\left(\frac{\alpha^{\ell}}{a^{\ell+1}}\right)\sum_{p=0}^{\ell}F_{\ell mp}(i)\sum_{q=-\infty}^{\infty}G_{\ell pq}(e)\cdot\frac{\partial S_{\ell mpq}(\omega,M,\Omega,\theta)}{\partial M} \tag{2-69f}$$

The derivatives of the functions $F_{lmp}(i)$, $G_{lpq}(e)$ and $S_{lmpq}(\omega, M, \Omega,\theta)$ still need to be evaluated. These derivatives are listed here:

$$\frac{\partial S_{\ell mpq}(\omega,M,\Omega,\theta)}{\partial \omega} = -C_{\ell m}(\ell-2p)\sin[(\ell-2p)\omega+(\ell-2p+q)M+m(\Omega-\theta)] \tag{2-70a}$$

$$\frac{\partial S_{\ell mpq}(\omega,M,\Omega,\theta)}{\partial \Omega} = -mC_{\ell m}\sin[(\ell-2p)\omega+(\ell-2p+q)M+m(\Omega-\theta)] \tag{2-70b}$$

$$\frac{\partial S_{\ell mpq}(\omega,M,\Omega,\theta)}{\partial M} = -C_{\ell m}(\ell-2p+q)\sin[(\ell-2p)\omega+(\ell-2p+q)M+m(\Omega-\theta)] \tag{2-70c}$$

(2-71)

$$\frac{dF_{\ell mp}(i)}{di} = \sum_{t}^{\min(p,k)} \frac{(2\ell-2t)!\sin^{\ell-m-2t}(i)\cos i}{t!(\ell-t)!(\ell-m-2t)!2^{2(\ell-t)}} \sum_{s=0}^{m}\binom{m}{s}\cos^{s} i \sum_{c=0}^{p-t}\binom{\ell-m-2t+s}{c}\binom{m-s}{p-t-c}(-1)^{c-k}$$

$$- \sum_{t}^{\min(p,k)} \frac{(2\ell-2t)!\sin^{\ell-m-2t}(i)}{t!(\ell-t)!(\ell-m-2t)!2^{2(\ell-t)}} \sum_{s=0}^{m}\binom{m}{s} s\cos^{s-1} i\sin i \sum_{c=0}^{p-t}\binom{\ell-m-2t+s}{c}\binom{m-s}{p-t-c}(-1)^{c-k}$$

$$\frac{dG_{\ell pq}(e)}{de} = (-1)^{|q|}\left(1+\beta^2\right)^{\ell}\beta^{|q|}\sum_{k=0}^{\infty}\left\{Q\beta^{2k}\frac{dP}{de} + P\beta^{2k}\frac{dQ}{de} + 2kPQ\beta^{2k-1}\frac{d\beta}{de}\right\} \tag{2-72a}$$

$$\frac{dP}{de} = \sum_{r=0}^{h}\binom{2p'-2\ell}{h-r}\frac{(-1)^r}{r!}\frac{(\ell-2p'+q')}{2}\cdot\frac{-er\left[1+\sqrt{1-e^2}\right]^{r-1}}{\sqrt{1-e^2}} \tag{2-72b}$$

$$\frac{dQ}{de} = \sum_{r=0}^{h}\binom{-2p'}{h-r}\frac{(-1)^r}{r!}\frac{(\ell-2p'+q')}{2}\cdot\frac{-er\left[1+\sqrt{1-e^2}\right]^{r-1}}{\sqrt{1-e^2}} \tag{2-72c}$$

$$\frac{d\beta}{de} = \frac{1}{1+\sqrt{1-e^2}} + \frac{e^2}{\sqrt{1-e^2}\left(1+\sqrt{1-e^2}\right)^2} \tag{2-72d}$$

3. Averaging Issues

Previous studies[14] have averaged the disturbing function over the mean anomaly for a single orbit, under the assumption that any short-period periodic perturbations will have no net effect after each revolution. This effectively reduces the model to the effects of any secular and long-period periodic variations. While this assumption may be acceptable for nearly spherical bodies such as the Earth and Moon, it is not as applicable to very nonspherical objects due to possible passes close to an elongated end of the asteroid, which could lead to large changes in the orbital elements. A side benefit of averaging the disturbing function is that the expression for the function "G" in Equation (2-63) is greatly simplified, and analytic answers are possible. Without this assumption, however, analytic solutions are much more difficult, if not impossible, to obtain.

Chapter III

Parametric Studies

With six orbital elements that can be varied, the space in which to search for suitable orbits is quite large. In the Keplerian problem, analytic solutions are possible, thereby lessening the numerical work significantly. For the problem considered here, however, an analytic solution is not as obvious (if one even exists). Therefore a variety of numerical techniques are employed. This chapter covers parametric studies that are used to study the properties of a large number of orbits by numerical integration.

A. Method Definition

Three asteroids were studied parametrically: Gaspra, Ida and Vesta. For each asteroid, a variety of initial conditions were chosen and numerically integrated in MATLAB for a simulated time of thirty days. A Runge-Kutta $4^{th}/5^{th}$ order numerical integrator with variable step size was used, with an integration tolerance of 10^{-9}. These simulations used the elliptic integral representation of the potential function as described in the previous chapter. This required the computation of the parameter κ as in Equation (2-10) which allows the numerical integrator to determine if the satellite has impacted the primary, as κ is positive when exterior to the primary, zero when on the surface, and negative when in the interior. As such, if κ becomes negative during the integration, the simulation is stopped and the orbit state variables to that point are returned as output. Without this feature, should the satellite orbit pass through the primary body, the integration time step becomes extremely small to more accurately model the large changes in potential associated with close proximity to the gravitational center. This small time step increases the necessary computer time drastically and makes it inconvenient to continue the integration beyond this point. From a mission design standpoint, any orbit that impacts the surface is usually not suitable. However, discovering orbits that "crash" is useful because regions to be avoided can be defined.

All orbits studied were initially circular ($e = 0$) and polar ($i = 90°$). The initial argument of periapsis, node angle, and true anomaly were all set to combinations of initial values of 0° and 90°. Note that orbits with initial elements of $\omega = 0°$, $\Omega = 0°$, and

$\nu = 90°$ produce the same initial conditions in Cartesian coordinates as orbits with $\omega = 90°$, $\Omega = 0°$, and $\nu = 0°$. Similarly, orbits with $\omega = 0°$, $\Omega = 90°$, and $\nu = 90°$ produce the same initial conditions as orbits with $\omega = 90°$, $\Omega = 90°$, and $\nu = 0°$. This is a consequence of setting the initial eccentricity to zero. The initial semimajor axis is varied, leading to a parametric study of the dynamics about the central body. The size of the orbit, determined by the semimajor axis, has a significant effect on its general behavior. For this study, it is started close to the surface of the asteroid and gradually increased to a large distance away, with a constant step size, but with additional steps added near resonance orbits and also near "promising" orbits. Resonance orbits, discussed further in subsequent chapters, are those orbits where the orbital period is commensurate or nearly commensurate with the rotational period of the asteroid. Small changes in the initial size of the orbit can have dramatic effects on the orbit, especially in the vicinity of resonance orbits.

Once the initial conditions have been chosen, they are integrated for a period of thirty days, producing a matrix containing the state elements at each time step along the integration. The state elements are then transformed to orbital elements at each step. A number of plots are generated for each orbit: eccentricity as a function of argument of periapsis (in polar coordinates) as well as semimajor axis, distance from the center, altitude, and inclination as functions of time. The maximum and minimum values of semimajor axis, eccentricity, and inclination over the course of the orbit are recorded, as is the time of surface impact if the satellite "crashes" into the asteroid.

B. Results

The next sections summarize data collected from a subset of orbits studied for each asteroid. The parametric results spanning all combinations of orbital elements are also discussed. Their relation to other aspects of the study is covered in Chapter VI.

1. Sample Orbits

i. 16 km Circular Polar Orbit about Gaspra

This orbit appears to be a promising orbit for mission design. Figure 3-1 shows the eccentricity as a function of argument of periapsis over the course of thirty days for this orbit. This figure is shown on a polar plot, with argument of periapsis as the angular component, and eccentricity as the radial component. A two-body solution would result in a single point on the plot, since both elements would remain constant. In this study, however, both can vary significantly. The amount of variation can be affected by the initial conditions, and a certain set of conditions might lead to a useful orbit. In Figure 3-1, it can be seen that the maximum eccentricity is approximately 0.176. In addition, the plot shows a somewhat symmetrical and approximately repeating pattern about the origin, indicating that, although these two orbital elements will vary, the variation in eccentricity is bounded during the time period considered.

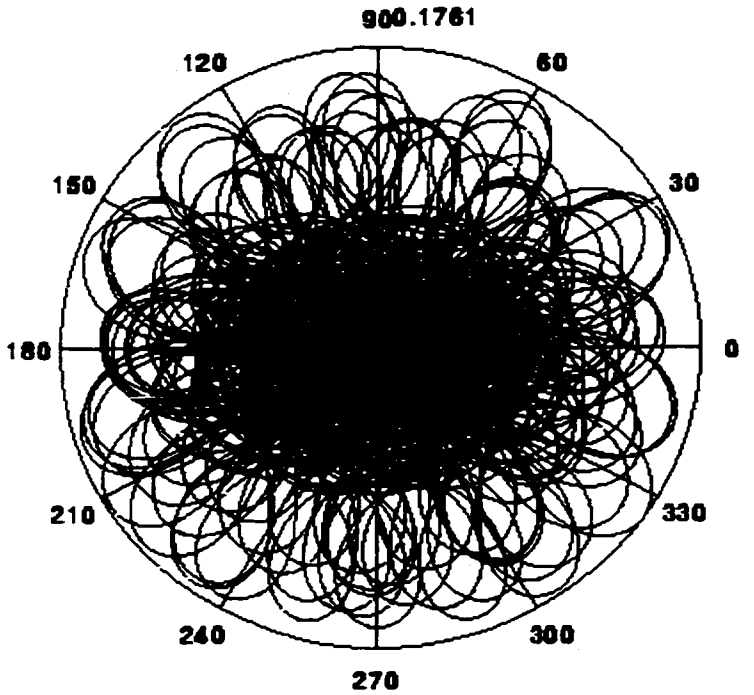

Figure 3-1. Eccentricity and Argument of Periapsis Progression, 16 km Polar Orbit about Gaspra

Figures 3-2 through 3-6 show the evolution of the semimajor axis, radial distance from the origin, altitude, eccentricity and inclination of the orbit over time, respectively. As with the eccentricity, all of these elements are bounded during this period of time. The altitude in particular is an important quantity since orbits with low altitudes can have a high probability of impacting the surface. A variation in altitude can be desirable, however, as it allows the surface to be studied under a variety of sensor resolutions.

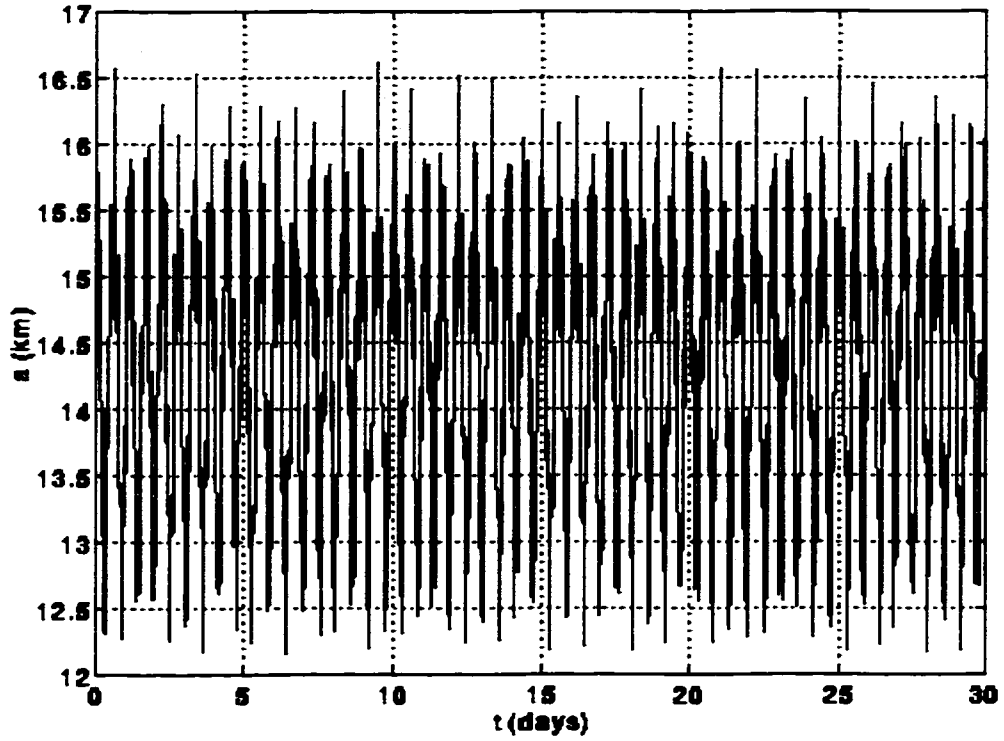

Figure 3-2. Semimajor Axis Progression, 16 km Polar Orbit about Gaspra

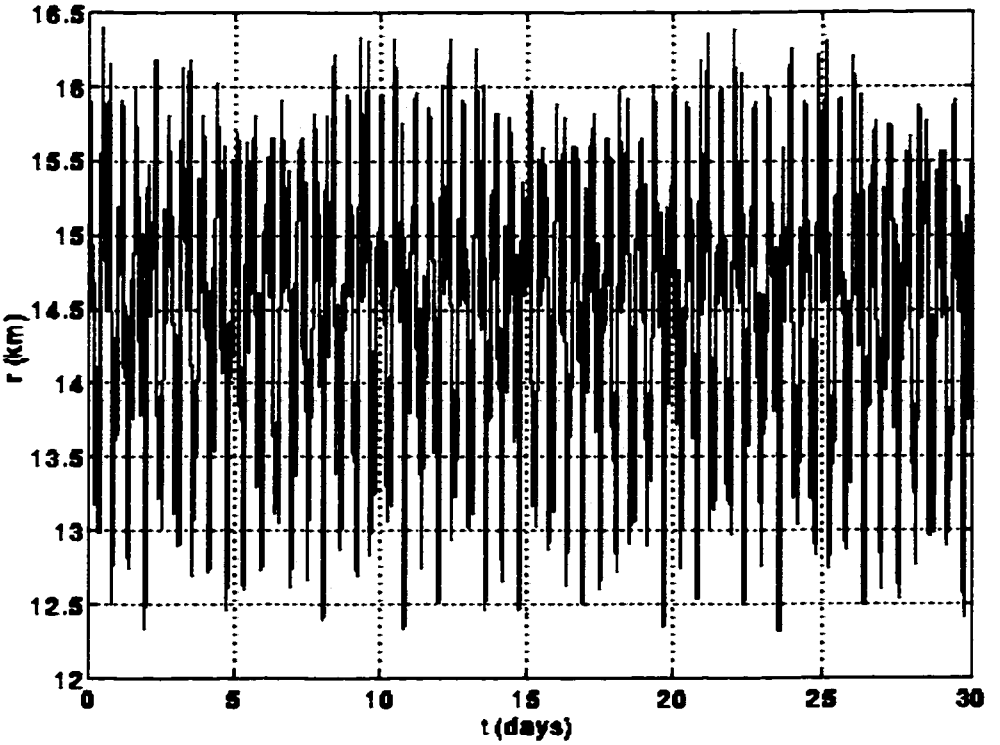

Figure 3-3. Radius Progression, 16 km Polar Orbit about Gaspra

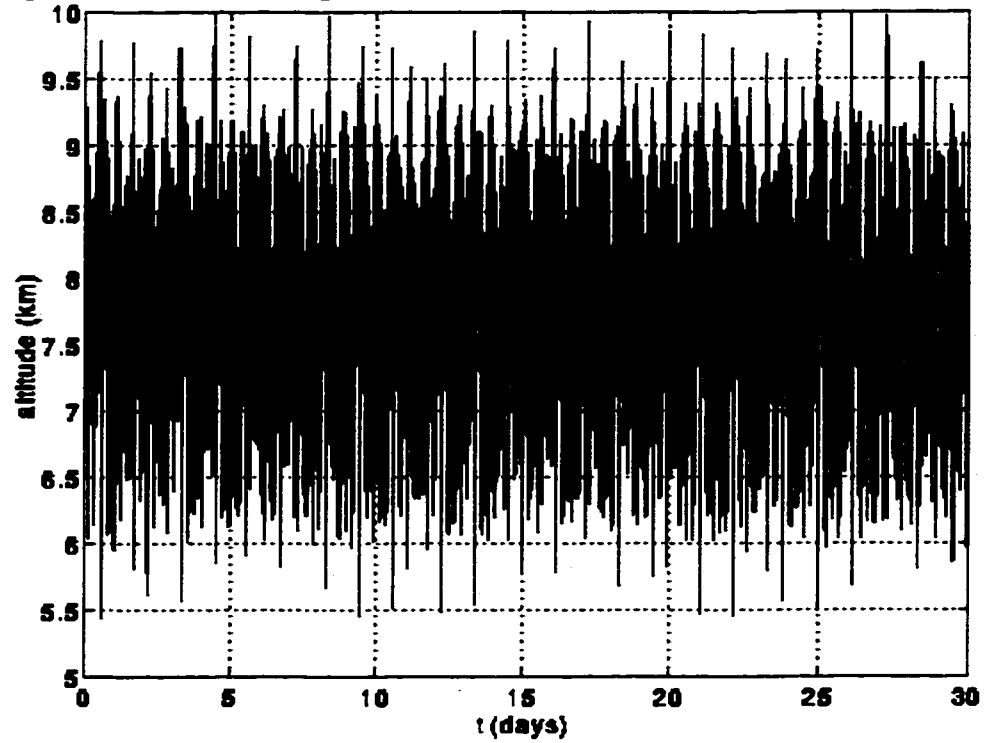

Figure 3-4. Altitude Progression, 16 km Polar Orbit about Gaspra

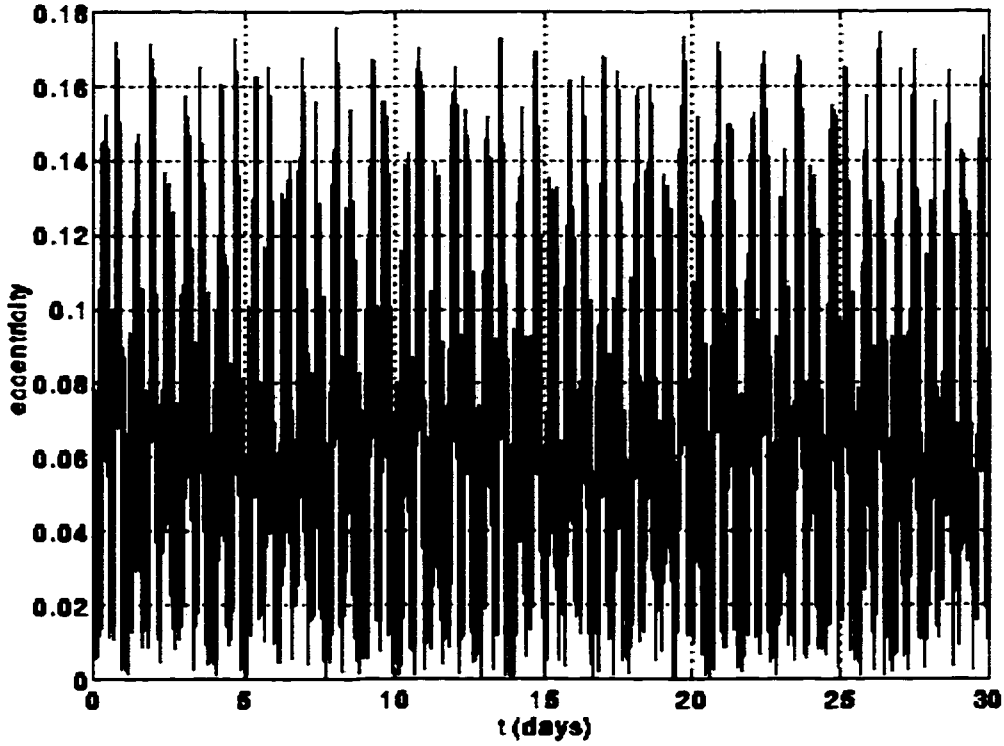

Figure 3-5. Eccentricity Progression, 16 km Polar Orbit about Gaspra

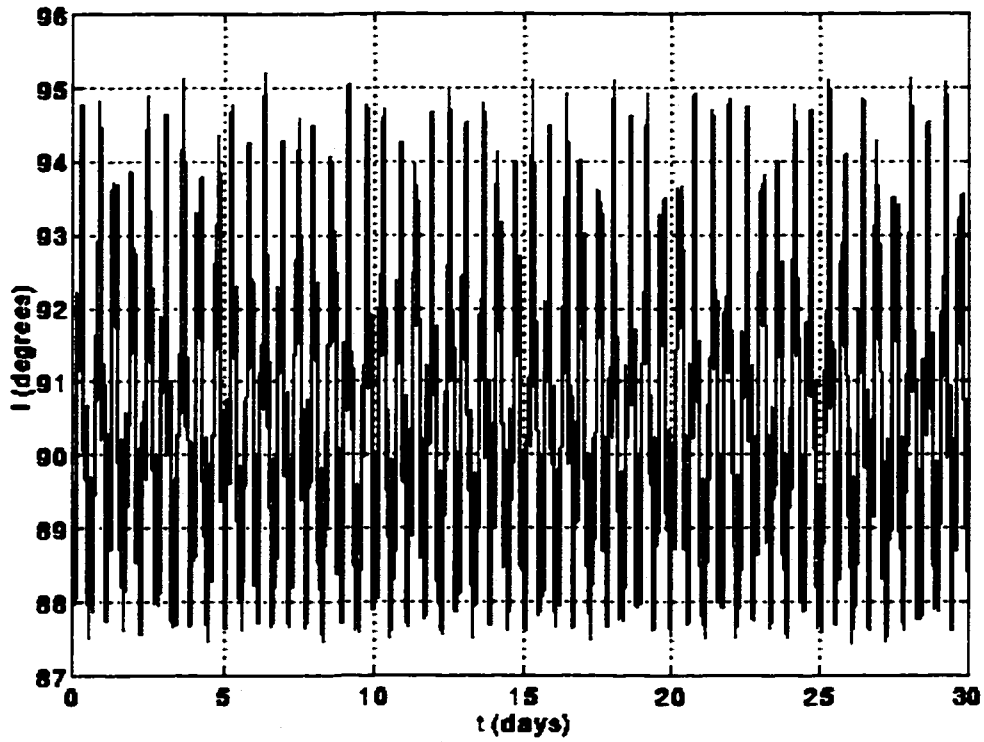

Figure 3-6. Inclination Progression, 16 km Polar Orbit about Gaspra

ii. Polar Orbits about Gaspra Near 16 km

Figures 3-7 through 3-10 show the progression of eccentricity and argument of periapsis for polar orbits about Gaspra with an initial semimajor axis of 15.75 km, 15.8 km, 16.1 km and 16.5 km, respectively. The initial semimajor axis can have a significant effect on the nature of the elements. As Figure 3-8 shows, a small decrease from 16 km does not change the nature very much. The eccentricity is still bounded, although the maximum value is larger, at 0.196, and the apparently semiperiodic nature is still present. However, a decrease to 15.75 km drastically changes the orbit as shown in Figure 3-7. For this orbit, the eccentricity appears to remain small for a period of time, but then fluctuates with the argument of periapsis, achieving a maximum eccentricity of almost 0.55. Similarly, Figure 3-9 shows that a small increase to 16.1 km also changes the nature of the orbit, in this case achieving a maximum eccentricity of 0.61. Finally, Figure 3-10 shows that a larger increase to 16.5 km changes the orbit so much that the maximum eccentricity is 0.95, which is nearly a hyperbolic orbit. In fact, the eccentricity seems to be increasing with time, so that the satellite may indeed achieve a hyperbolic orbit and possibly escape sometime after thirty days.

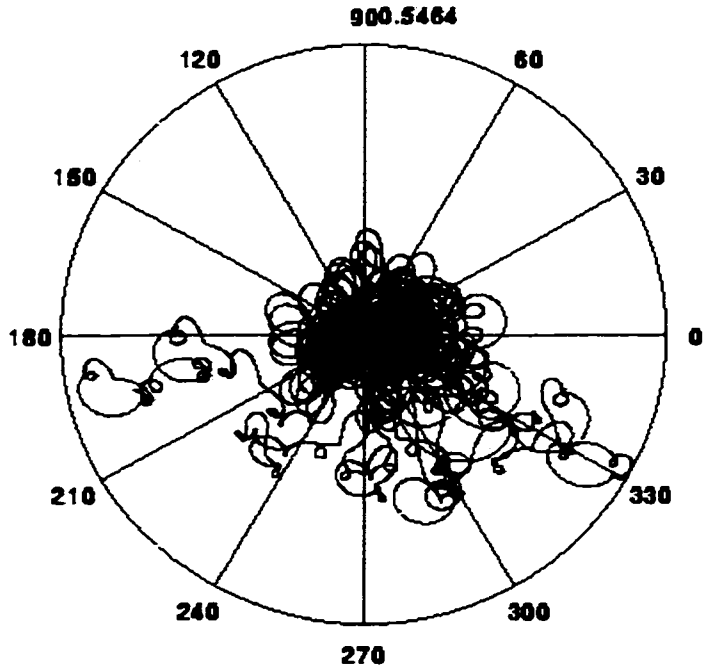

Figure 3-7. Eccentricity and Argument of Periapsis Progression, 15.75 km Polar Orbit about Gaspra

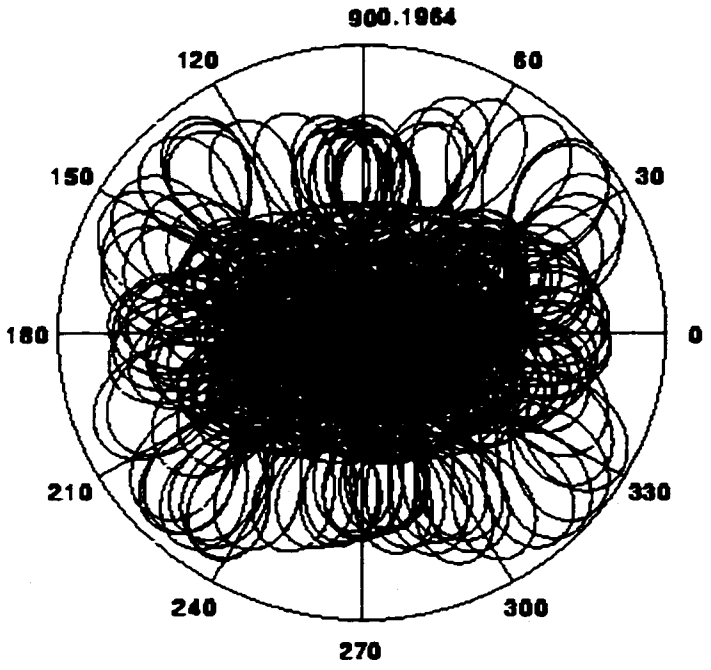

Figure 3-8. Eccentricity and Argument of Periapsis Progression, 15.8 km Polar Orbit about Gaspra

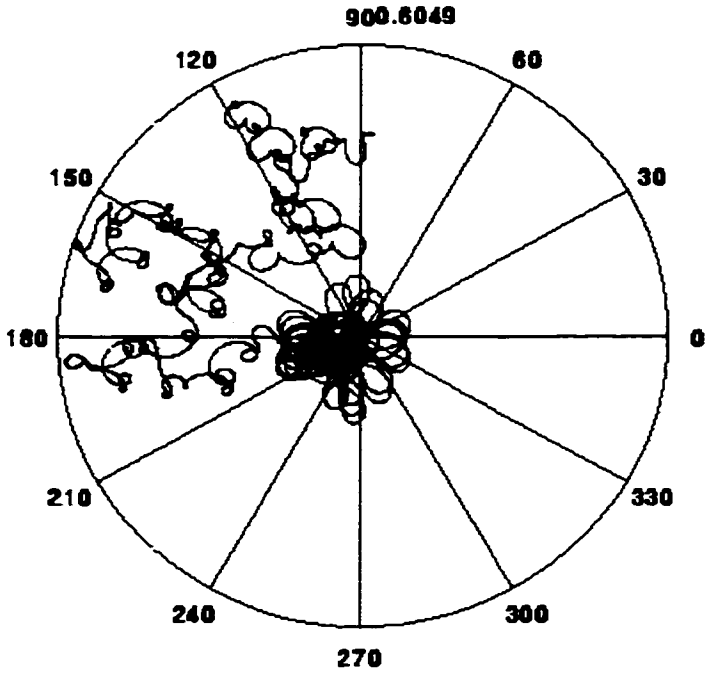

Figure 3-9. Eccentricity and Argument of Periapsis Progression, 16.1 km Polar Orbit about Gaspra

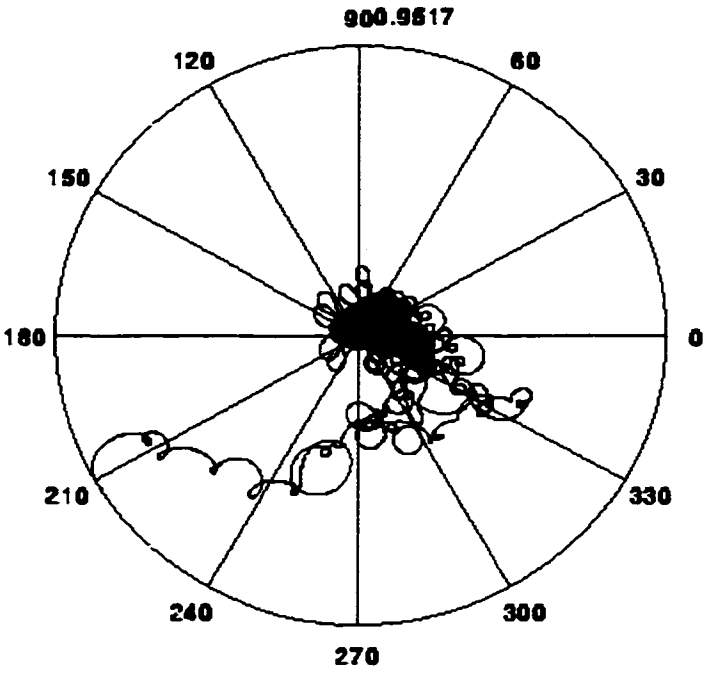

Figure 3-10. Eccentricity and Argument of Periapsis Progression, 16.5 km Polar Orbit about Gaspra

iii. Polar Orbits about Ida Near 47 km

Figures 3-11 through 3-15 show the polar plots for orbits about Ida with semimajor axis values of 46 km, 46.5 km, 47 km, 47.5 km and 48 km, respectively. These plots were generated with initial conditions of $i = 90°$, $e = 0$, $\omega = \Omega = 0°$ and $\nu = 90°$. Like Figure 3-1, eccentricity is plotted as the radial component of the polar plot, while argument of periapsis is the angular component. Again, a small change in the initial semimajor axis produces a large change in the nature of this plot. In Figure 3-11, which corresponds to the 46.0 km orbit, the eccentricity remains bounded for a time, but eventually achieves a maximum value of approximately 0.80, which is highly eccentric. In addition, the eccentricity appears to be increasing at the thirty day point of the orbit, suggesting the orbit may eventually become hyperbolic. However, in Figure 3-12, which corresponds to the 46.5 km orbit, the eccentricity remains more tightly bounded throughout the first thirty days. Here, the maximum eccentricity is nearly 0.11, much smaller than in the previous case. In Figure 3-13 and Figure 3-14, for the 47.0 km and 47.5 km orbits, respectively, the maximum eccentricity is also rather small, at 0.13 and 0.11, respectively. When the semimajor axis is further increased to 48.0 km, as shown in Figure 3-15, the orbit again becomes highly eccentric, achieving a maximum eccentricity of 0.94.

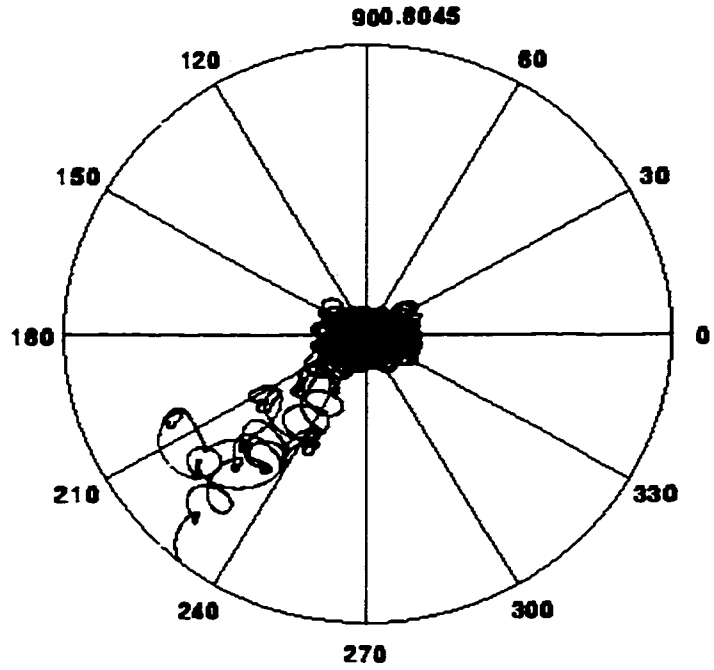

Figure 3-11. Eccentricity and Argument of Periapsis Progression, 46 km Polar Orbit about Ida

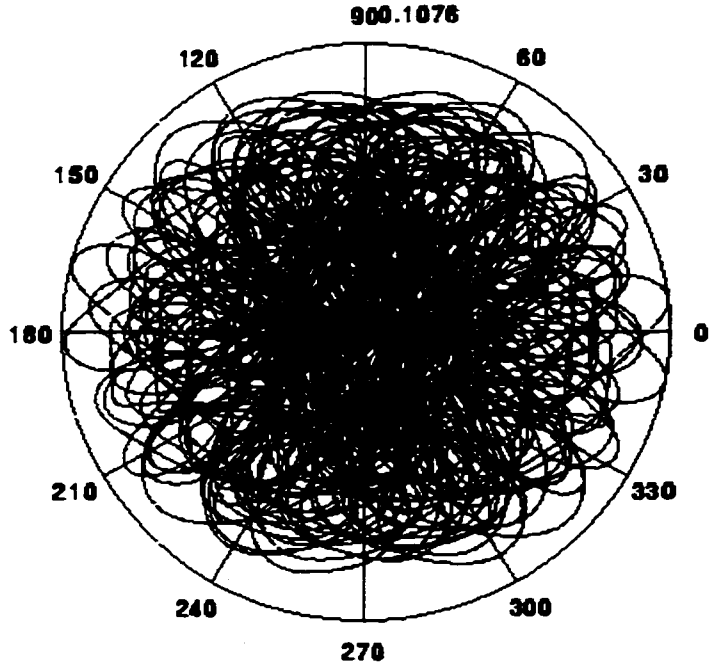

Figure 3-12. Eccentricity and Argument of Periapsis Progression, 46.5 km Polar Orbit about Ida

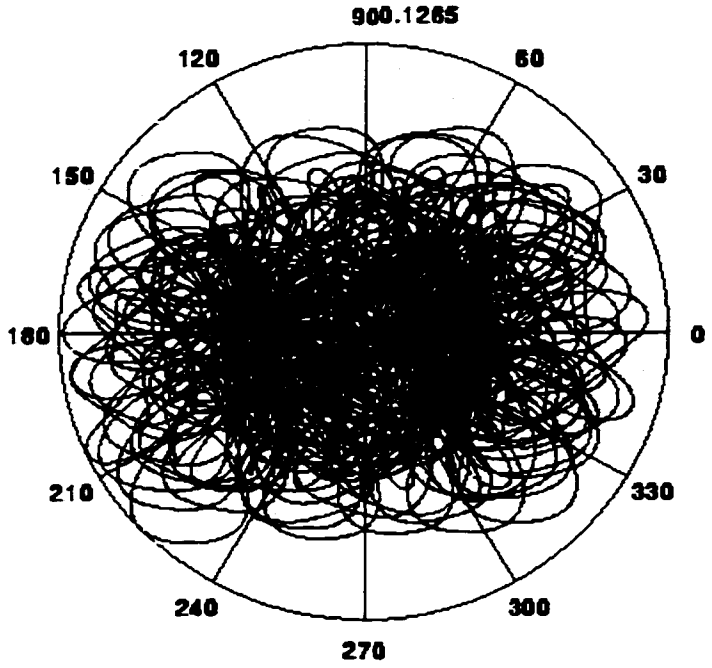

Figure 3-13. Eccentricity and Argument of Periapsis Progression, 47 km Polar Orbit about Ida

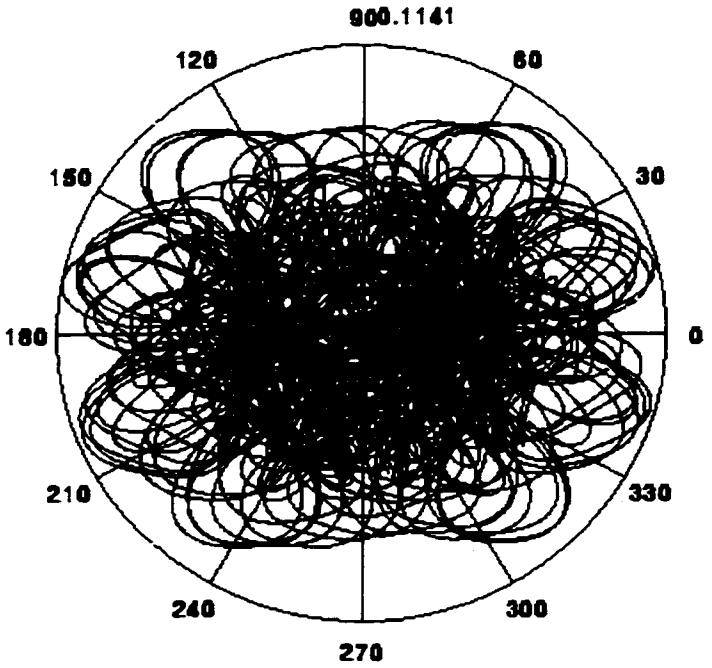

Figure 3-14. Eccentricity and Argument of Periapsis Progression, 47.5 km Polar Orbit about Ida

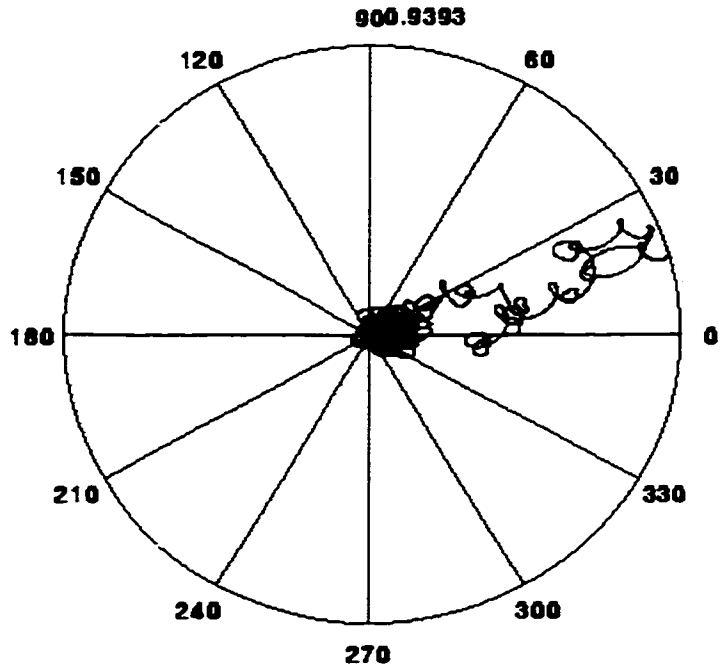

Figure 3-15. Eccentricity and Argument of Periapsis Progression, 48 km Polar Orbit about Ida

2. Parametric Studies

The previous section showed polar plots for some specific orbits, with one orbit shown on each plot. The results of the parametric studies are presented next. These studies allow the viewing of the properties of a number of different orbits on one plot.

i. Gaspra

Figures 3-16 through 3-18 show the results of a number of simulations about Gaspra, with each simulation covering a time period of thirty days as in the previous sections. These figures show the parametric results of these studies. The initial conditions are set at $e = 0$, $i = 90°$, $\omega = 0°$, $\Omega = 0°$ and $90°$, and $\nu = 0°$ and $90°$. The effect of the initial semimajor axis is the primary focus of this study, and so is varied from close to the asteroid (14 km) to relatively far away (25 km) in steps of 0.5 km, with smaller steps near points of interest, such as apparently stable orbits and resonance orbits. The variations of the semimajor axis, eccentricity, and inclination (i.e., the difference between the largest

and smallest values) are then plotted in Figure 3-16, Figure 3-17, and Figure 3-18, respectively.

At semimajor axis values less than 22 km, the orbits are quite erratic. The 16 km orbit with $\Omega = 0°$ and $\nu = 0°$ is seen to have small changes in the orbital elements, while the surrounding orbits have relatively large variations. There are other examples of this, such as the 18 km and 19 km orbits with $\Omega = 90°$, and $\nu = 90°$, and the 17.5 km orbit with $\Omega = 90°$, and $\nu = 0°$.

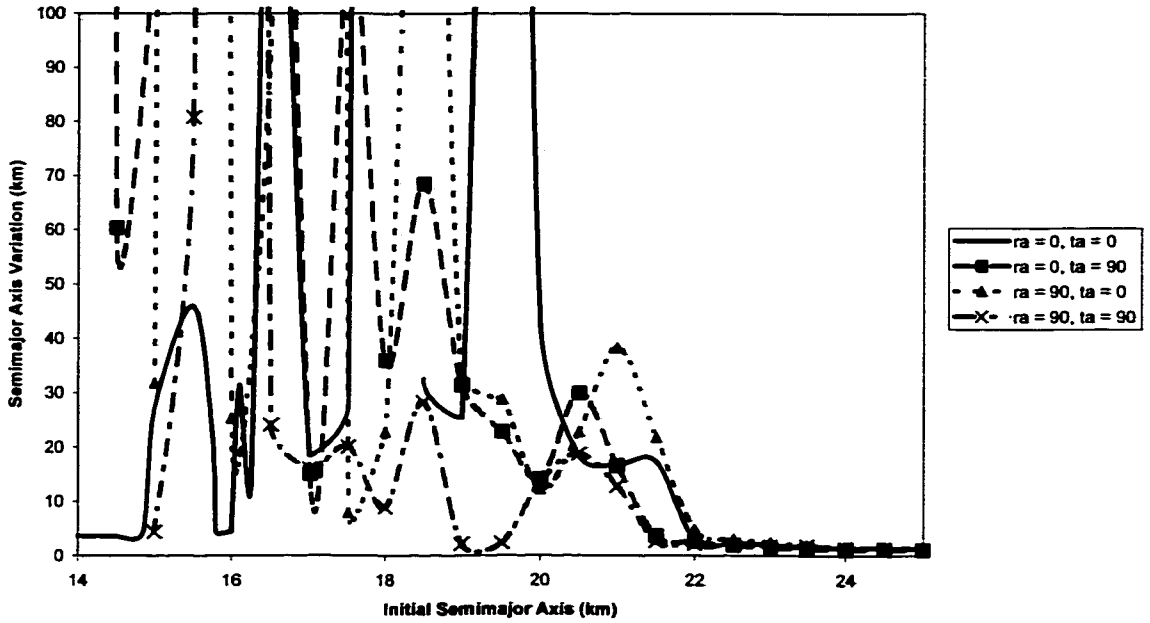

Figure 3-16. Semimajor Axis Variation for Gaspra

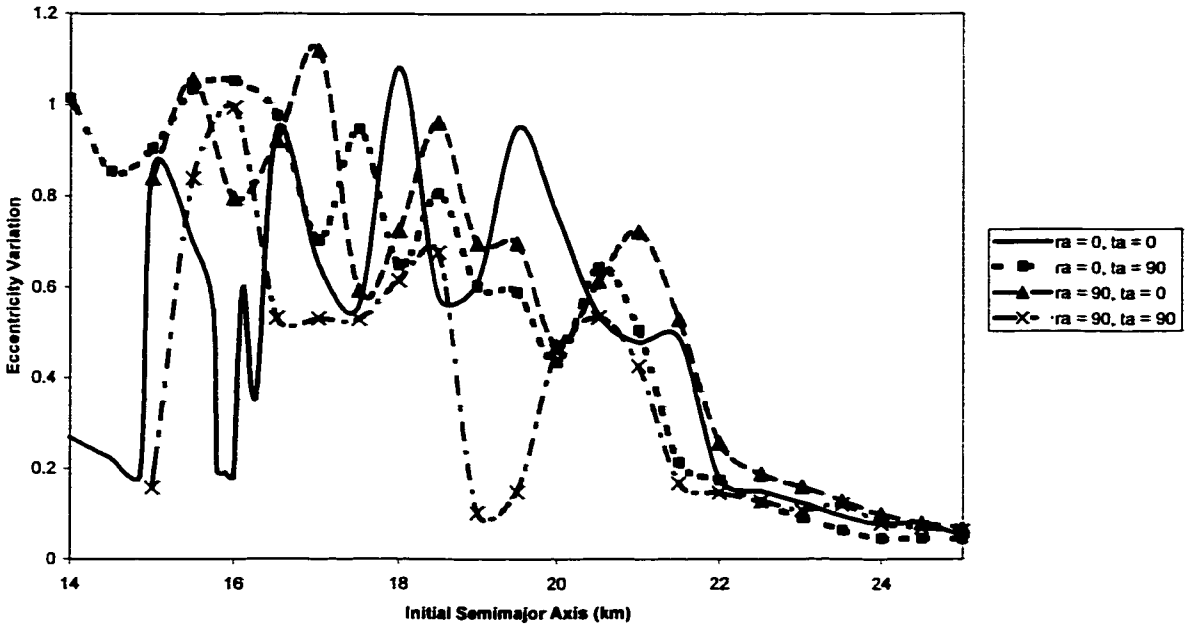

Figure 3-17. Eccentricity Variation for Gaspra

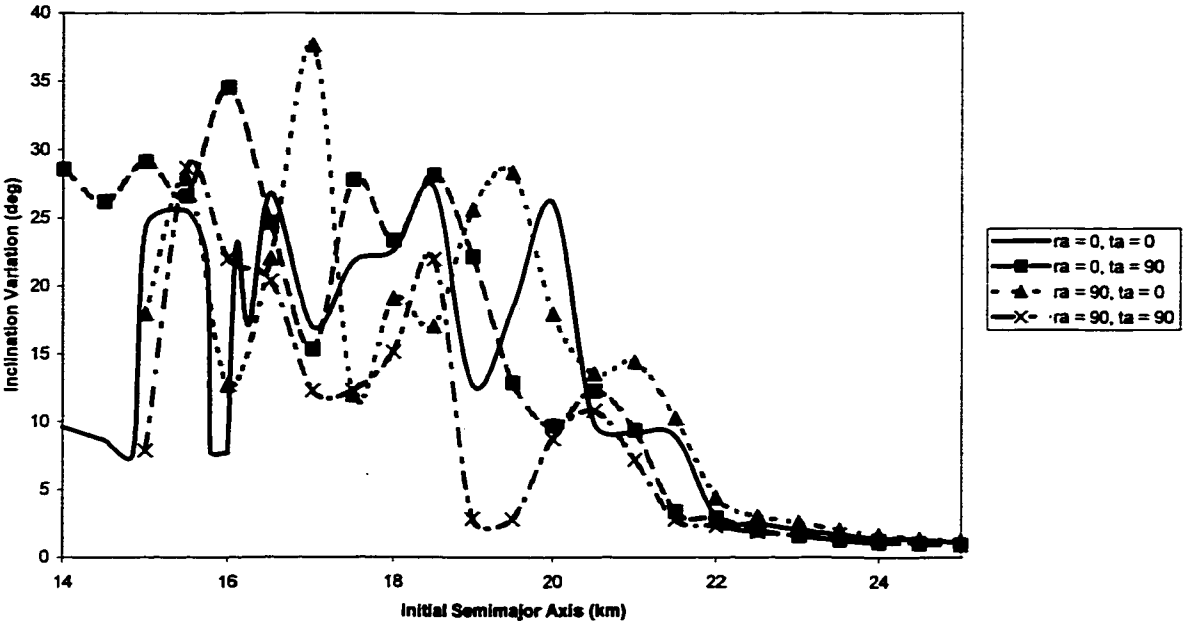

Figure 3-18. Inclination Variation for Gaspra

ii. Ida

Figures 3-19 through 3-21 show the variations for semimajor axis, eccentricity, and inclination, respectively, for Ida. These charts show that orbits below 55 km tend to have large changes in the orbital elements, while those above 55 km have small changes.

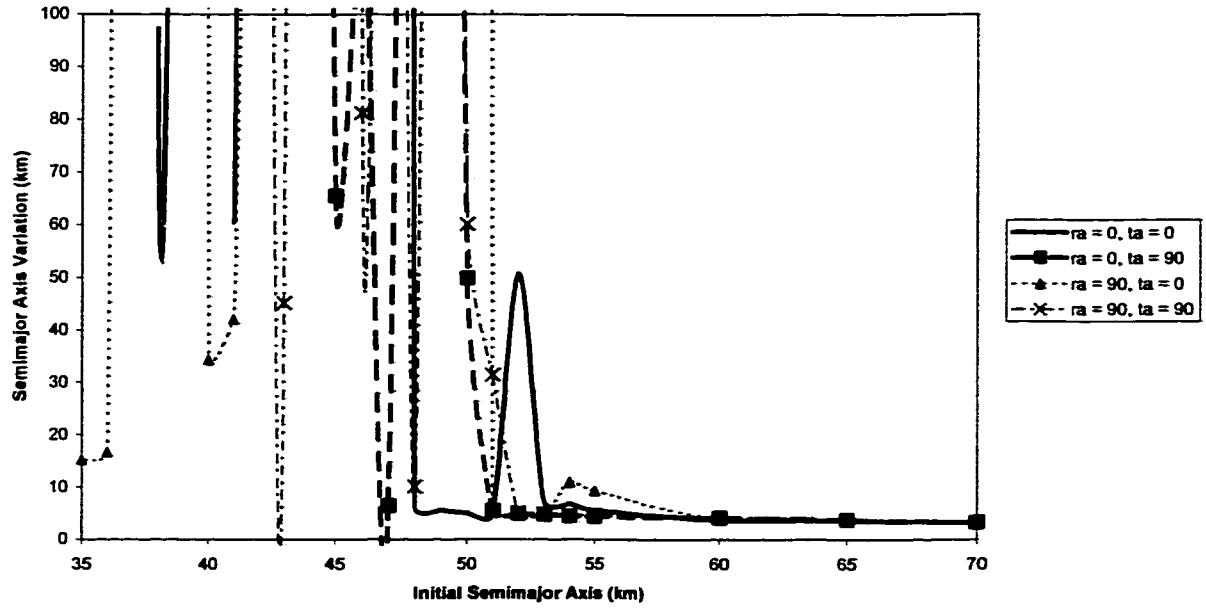

Figure 3-19. Semimajor Axis Variation for Ida

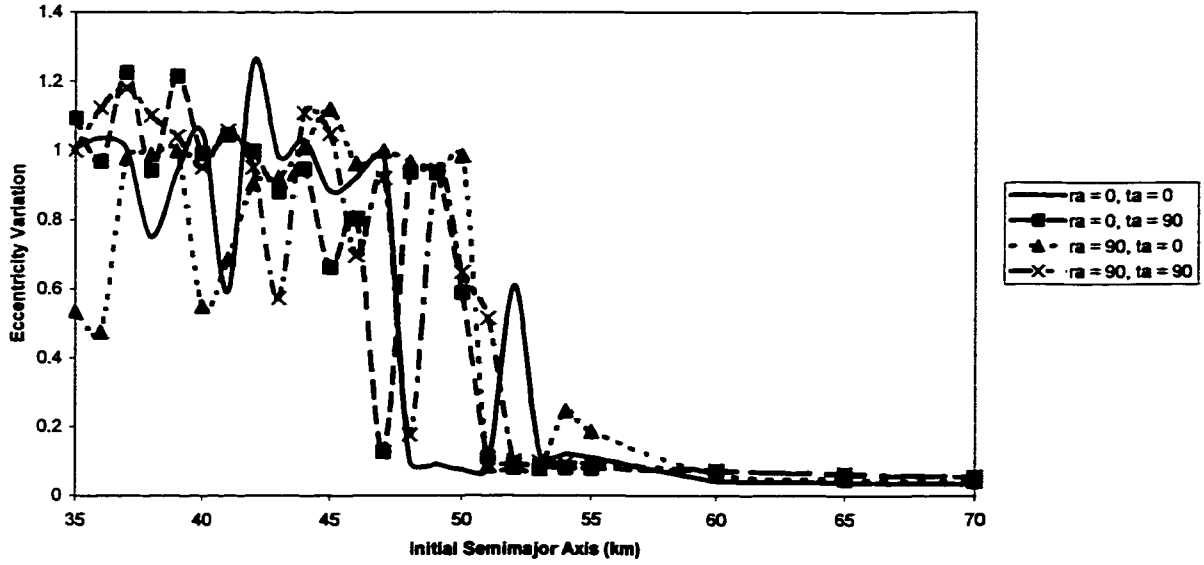

Figure 3-20. Eccentricity Variation for Ida

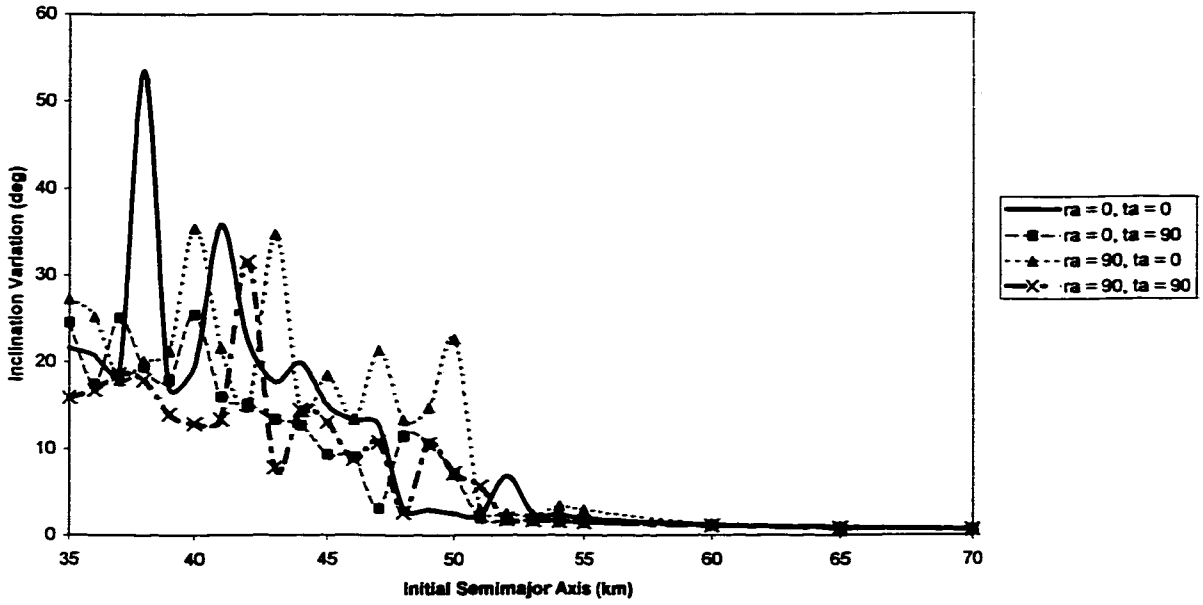

Figure 3-21. Inclination Variation for Ida

iii. Vesta

Figures 3-22 through 3-24 show the variations for the semimajor axis, eccentricity, and inclination, respectively, for Vesta. These charts show that orbits below 800 km tend to have large changes in the orbital elements, while those above 800 km have small changes.

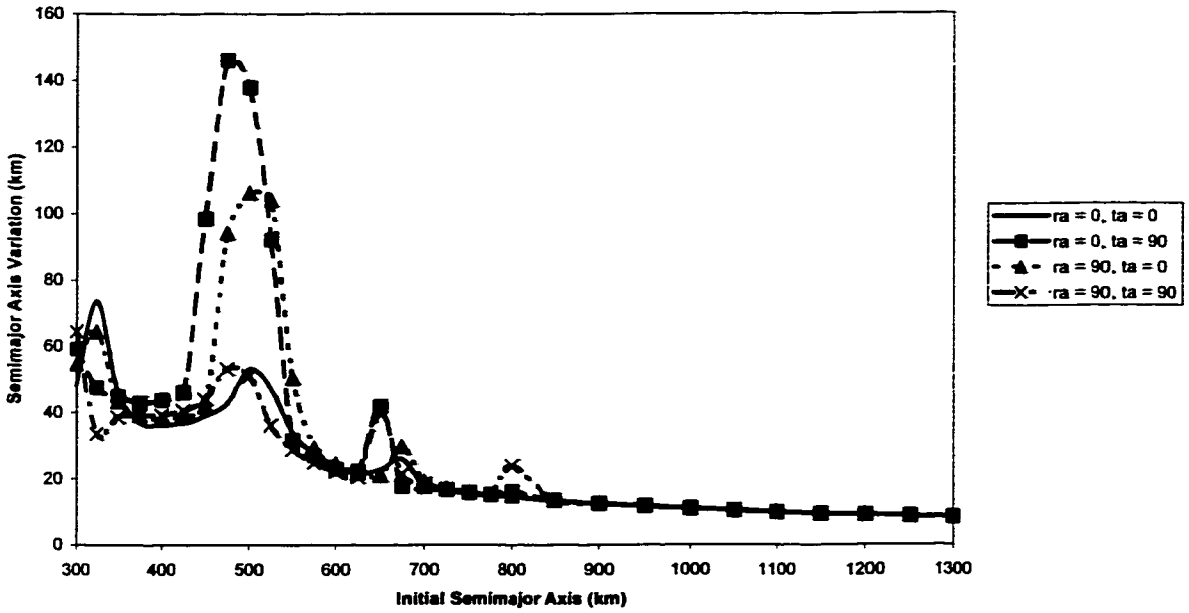

Figure 3-22. Semimajor Axis Variation for Vesta

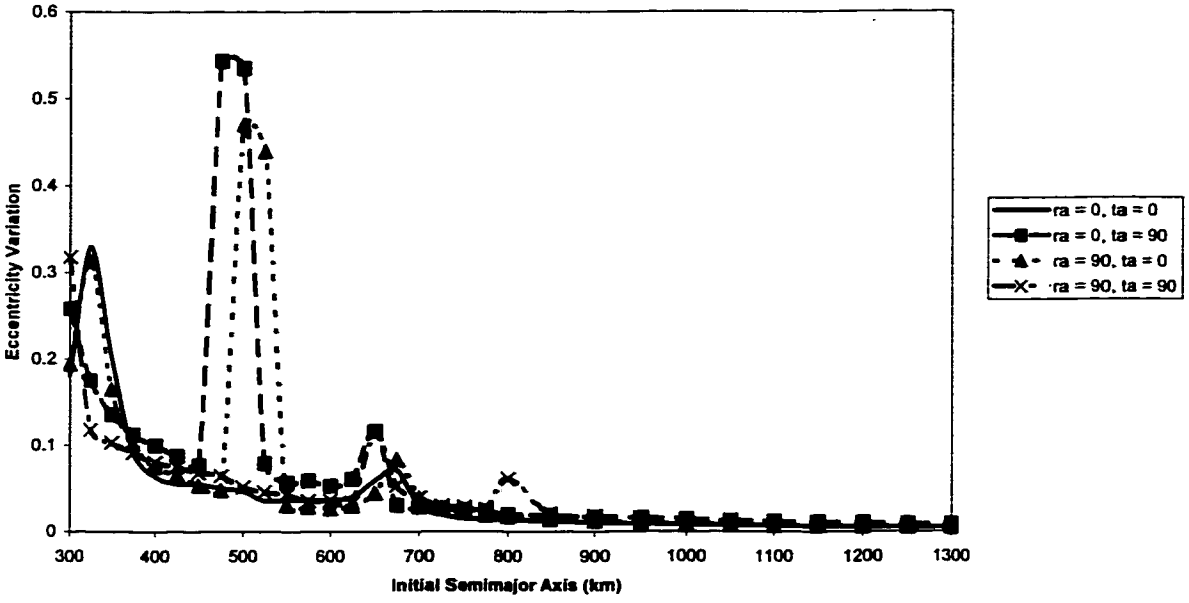

Figure 3-23. Eccentricity Variation for Vesta

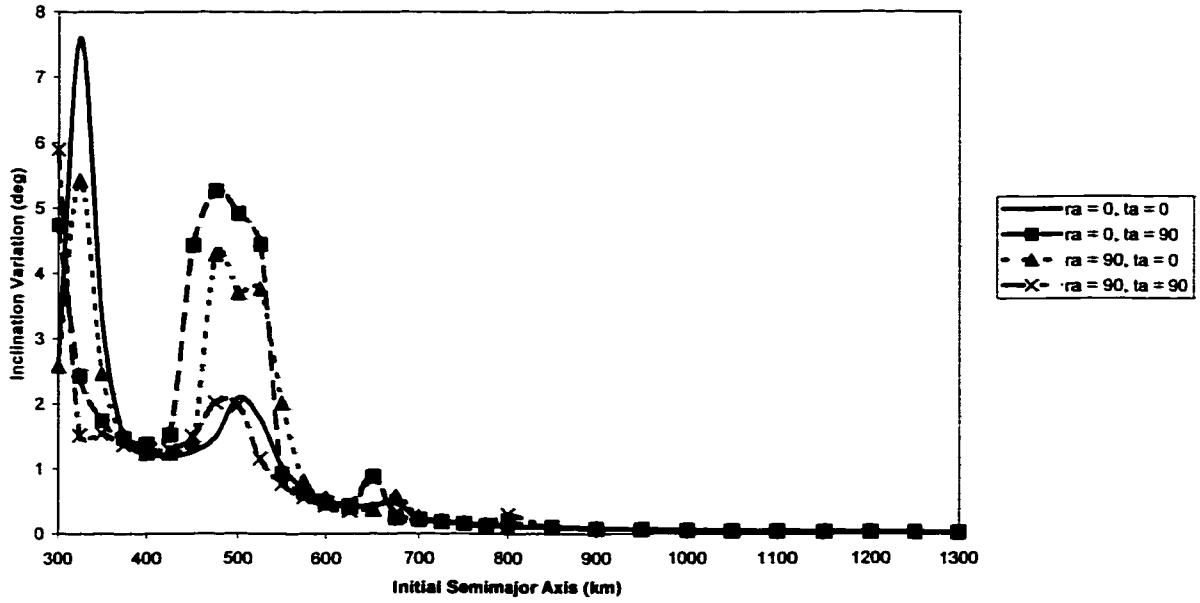

Figure 3-24. Inclination Variation for Vesta

C. Conclusion

The orbital element plots parametric studies show promise for analyzing the different orbital regions. The parametric studies especially allow study of a wide variety of initial conditions on one plot. Additionally, some regions in the parametric plots show "jumps" in the orbital element variations compared to the surrounding orbits. For example, in Figures 3-22 through 3-24, there are large variations near semimajor axis values of 500 km, 650 km and 800 km. The 500 km region roughly corresponds to the 1:1 resonance area, the 650 km to the 3:2 resonance, and the 800 km to the 2:1 resonance. These areas will be further studied in discussion of the differential correction algorithms.

Chapter IV

Resonance Orbit Periapsis Plots

The parametric studies presented in the previous chapter provide a way to study a large number of orbits simultaneously. The remainder of this study consists of methods that focus on a smaller number of orbits to better understand each case in more detail. This chapter covers what will be called "periapsis plots," or plots of the rate of change of the periapsis distance over the course of the orbit. Resonance orbits will be studied in particular because of the possible beneficial effects resonance can induce. These studies will be used in conjunction with the differential corrections presented in the following chapter.

A. Definition

Those orbits in which the orbital period is a small integer multiple of the rotational period of the asteroid are termed "resonance" orbits. These orbits can have unique dynamic properties since the orbit of the satellite may be approximately periodic in the rotating reference frame. The orbit will not be truly periodic due to the highly nonspherical shape of the asteroid, but may provide a sufficient initial estimate for the differential corrections method presented later. First, estimates of the orbit sizes for some of the resonance orbits for each satellite in this study are produced, and the resulting orbits are numerically integrated. Then Lagrange's Planetary Equations are used to calculate dr_p/dM for each time interval, where r_p is the radius of periapsis, and the results plotted as a function of the argument of latitude. These plots will be referred to as "periapsis plots" for the remainder of this paper.

These results are used in an attempt to predict which resonance orbits are unlikely to escape or crash into the asteroid. A differential correction technique is applied to produce initial conditions for an orbit that is nearly periodic with respect to the rotating frame. An attempt is made to correlate the convergence of the differential corrections and the symmetry (or the lack thereof) of the periapsis plots.

Table 4-1 shows the approximate resonance orbit sizes for the asteroids considered in this study. The results are approximate because the Keplerian equation $P = 2\pi\sqrt{a^3/\mu}$ was used to estimate the period of the orbit based on the semimajor axis.

Table 4-1. Approximate Resonance Orbit Sizes

Asteroid	Resonance	Orbit Period (hrs)	Estimated Orbit Size (km)
Gaspra	1:1	7.0	17
	2:1	14.0	27
	3:1	21.0	35
	4:1	28.0	43
Eros	1:1	5.27	20
	2:1	10.54	32
	3:1	15.81	42
	4:1	21.08	50
Ida	1:1	4.63	29
	2:1	9.26	46
	3:1	13.89	60
	4:1	18.52	73
Vesta	1:1	5.3	508
	2:1	10.6	807
	3:1	15.9	1060
	4:1	21.2	1281

B. Sample Orbits

As one example, Figure 4-1 shows ten orbits revolutions for the Vesta 1:1 orbit size shown in Table 4-1 with respect to the rotating reference frame. Figure 4-2 shows the same orbit, but relative to the inertial reference frame. The exact initial conditions are given in Table 4-2. Note that the state variables are given with respect to the rotating reference frame.

Table 4-2. Vesta Estimated 1:1 Orbit Initial Conditions

Orbital Element	Initial Value	State Variable	Initial Value
a (km)	508.48	x (km)	508.48
e	0	y (km)	0
i (deg)	90	z (km)	0
ω (deg)	0	$\dot{x}$ (km/s)	0
Ω (deg)	0	$\dot{y}$ (km/s)	-0.167446
ν (deg)	0	$\dot{z}$ (km/s)	-0.167446

As seen in the figure, the orbit "drifts" in both frames. The orbit remains close to circular throughout the integration time, but the biggest influence appears to be a drift in the line of nodes. When the initial conditions are used in the orbit conditioning and differential correction algorithm presented later, however, the effect of this drift will be much smaller.

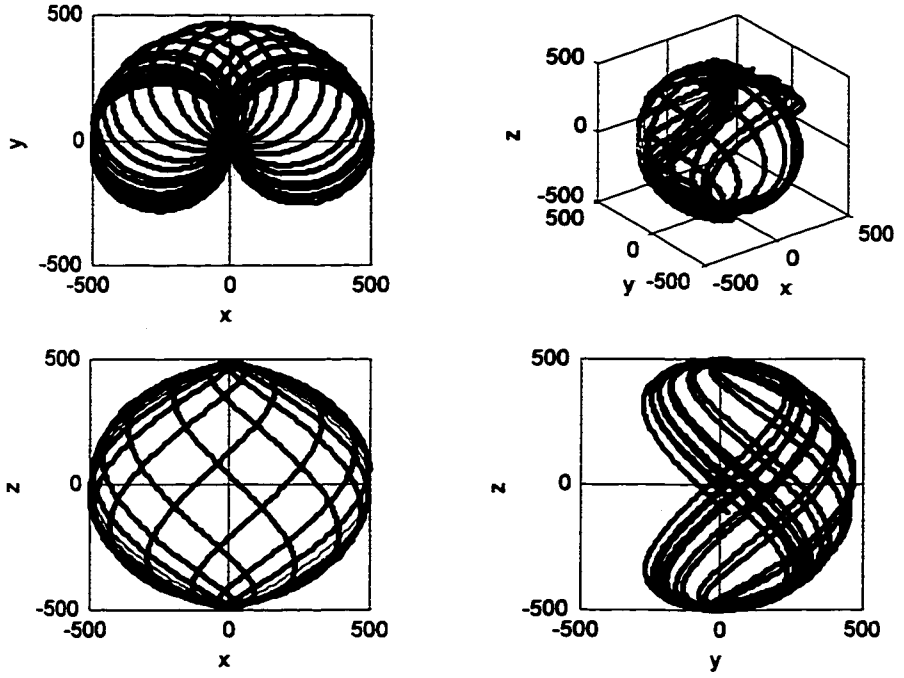

Figure 4-1. Vesta Estimated 1:1 Orbit in the Rotating Frame
10 revolutions shown

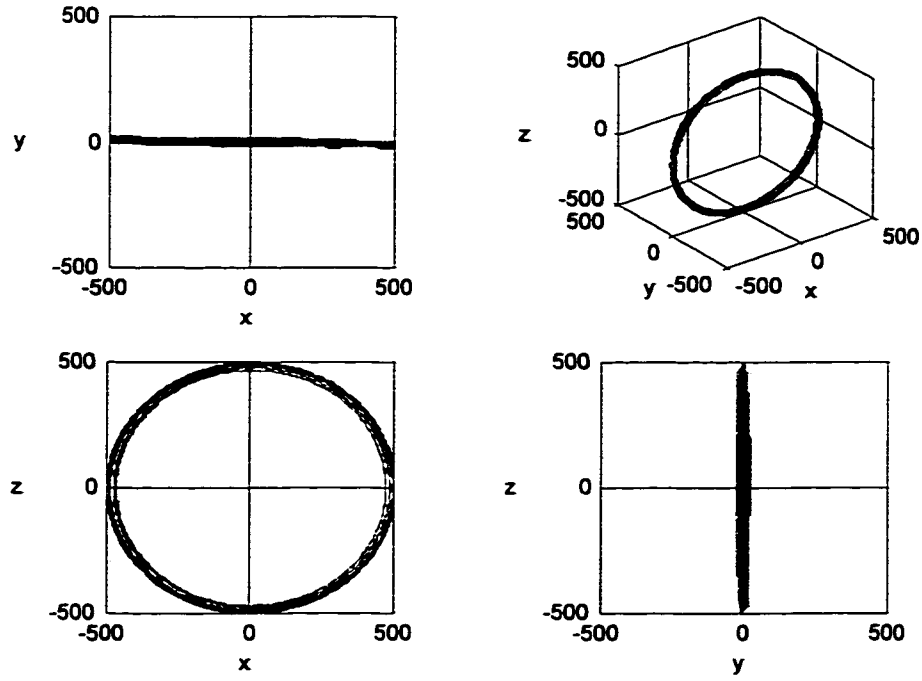

Figure 4-2. Vesta Estimated 1:1 Orbit in the Inertial Frame
10 revolutions shown

C. Periapsis Plots

Once an orbit has been integrated, the orbital elements can be calculated at each time step from the corresponding Cartesian coordinates. Lagrange's Planetary Equations can then be used in the forms presented in Chapter II to calculate dr_p/dM:

$$r_p = a(1-e) \tag{4-1}$$

$$\frac{dr_p}{dM} = \frac{da}{dM}(1-e) - a\frac{de}{dM} \tag{4-2}$$

where

$$\frac{da}{dM} = \frac{da/dt}{dM/dt} \tag{4-3}$$

$$\frac{de}{dM} = \frac{de/dt}{dM/dt} \tag{4-4}$$

with the derivatives da/dt, de/dt, and dM/dt calculated as shown in Chapter II.

As an example, consider Figure 4-3, which shows the value of dr_p/dM as the satellite completes one revolution, for the estimated 2:1 resonance orbit about Gaspra. Some symmetry is evident between the two halves of the orbit ($0 < L < \pi$ and $\pi < L < 2\pi$). Two asymptotes occur near $L = 7\pi/8$ and $L = 9\pi/8$. At these points dr_p/dM becomes infinitely large. This could indicate some kind of sensitivity in the dynamic model at these points, with large changes in r_p. However, since there are two asymptotes, symmetrically spaced around $L = \pi$, the overall net effect seems to be that the changes in periapsis cancel. Thus, if these individual changes are not too great (resulting in crash or escape), then the orbit shows promise. Figure 4-4 shows a similar plot for the estimated 3:1 orbit. The nature of this plot is different from Figure 2 in that there appears to be no infinite values for this orbit. Figure 4-5 shows the plot for the estimated 4:1 orbit. As with Figure 4-3, there are two regions where the change in periapsis distance seems to approach infinity.

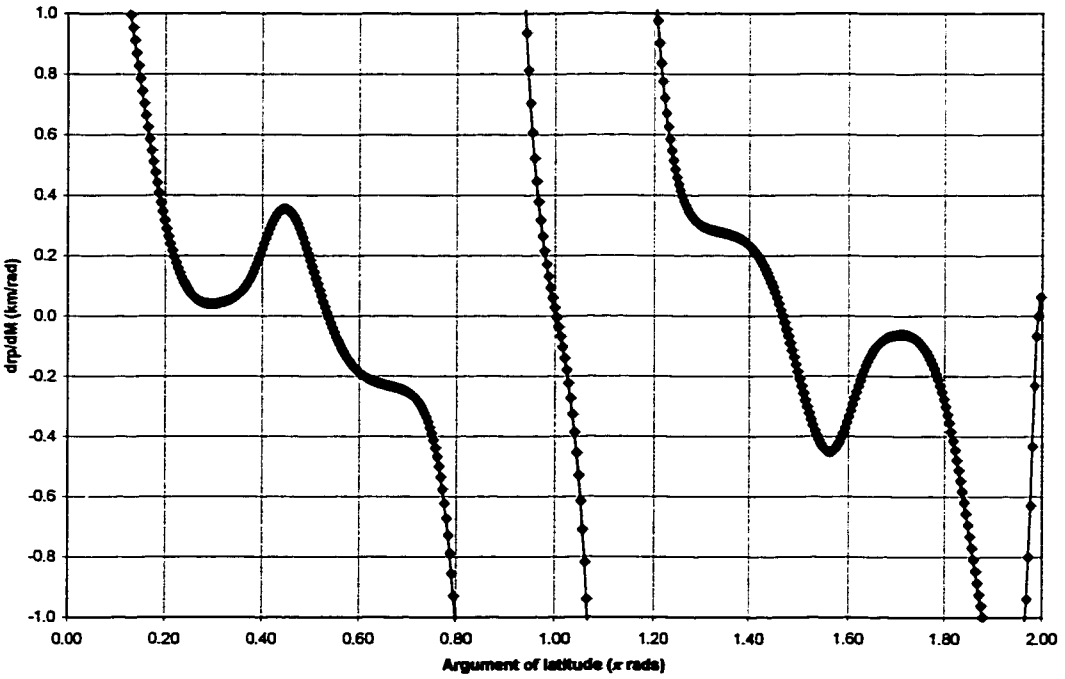

Figure 4-3. dr_p/dM for Estimated Gaspra 2:1 Resonance Orbit
a = 27.022 km, polar orbit

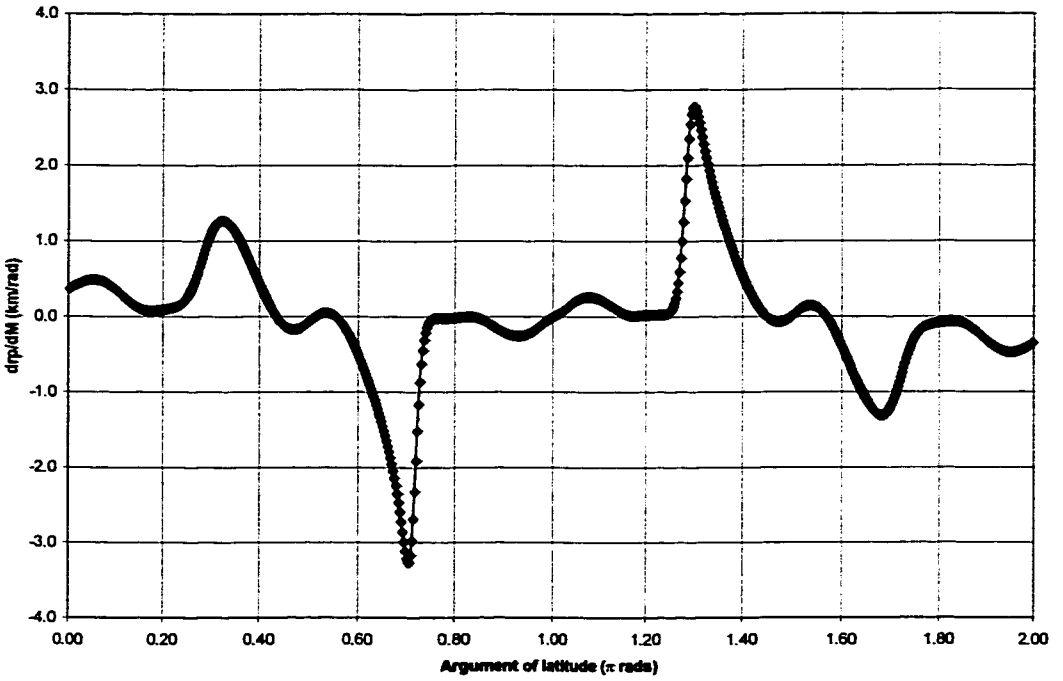

Figure 4-4. dr_p/dM for Estimated Gaspra 3:1 Resonance Orbit
a = 35.409 km, polar orbit

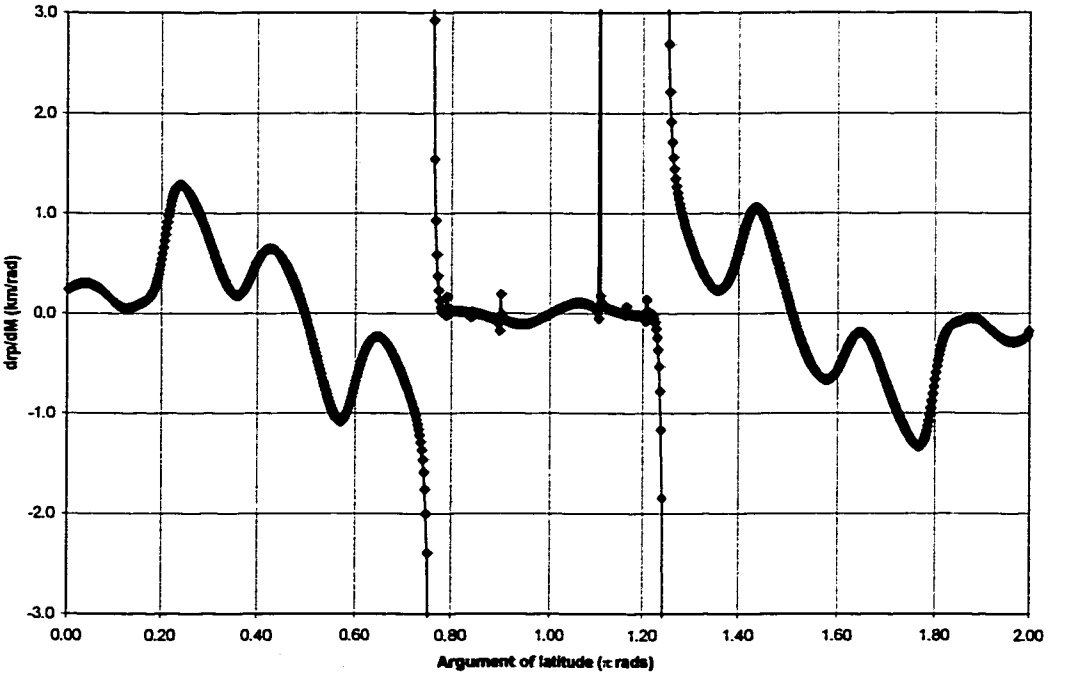

Figure 4-5. dr_p/dM for Estimated Gaspra 4:1 Resonance Orbit
a = 42.895 km, polar orbit

Figure 4-6 shows the periapsis plot for the estimated 1:1 resonance orbit about Vesta, corresponding to the orbit shown in Figures 4-1 and 4-2. This plot is similar to the Gaspra 3:1 orbit, in that there are no infinite values during the first revolution.

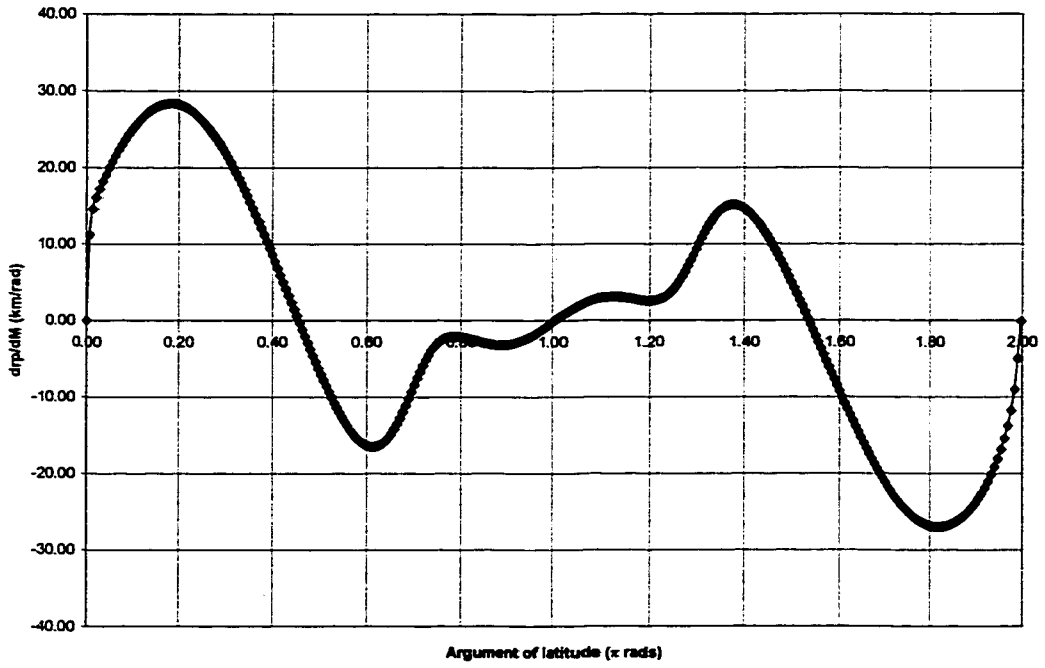

Figure 4-6. dr_p/dM for Estimated Vesta 1:1 Resonance Orbit
a = 508.48 km, polar orbit

D. Conclusion

This chapter has presented a method for calculating the rate of change of periapsis distance as a function of mean anomaly over the course of one orbit. The results tend to be symmetric in nature. This may be due to the symmetric nature of the model used as well as the resonant nature of the orbits chosen.

Chapter V

Differential Corrections and Orbit Conditioner

The previous sections concerned parametric studies of orbits and the nature of some resonance orbits. In this section, these orbits are modified in order to find *periodic* (or nearly periodic) orbits about asteroids, by using differential corrections.

Differential corrections can be used to find the initial conditions necessary to achieve a set of conditions at some point in the future (i.e., the "target conditions"). This type of process can be used in many different applications and is not limited to orbital mechanics. In this study, the algorithm is used in an attempt to determine the initial conditions, analogous to the orbital elements, needed to achieve a periodic orbit about an asteroid. So given the initial conditions at $t = t_0$

$$\overline{x}_0 = \begin{Bmatrix} x_o \\ y_o \\ z_o \\ \dot{x}_o \\ \dot{y}_o \\ \dot{z}_o \end{Bmatrix} \tag{5-1}$$

the target condition to meet is that the state variables at one revolution $t = t_1$, are to be identical to the initial conditions:

$$\overline{x}_1 = \overline{x}_0 \tag{5-2}$$

or, identically,

$$\begin{Bmatrix} x_1 \\ y_1 \\ z_1 \\ \dot{x}_1 \\ \dot{y}_1 \\ \dot{z}_1 \end{Bmatrix} = \begin{Bmatrix} x_o \\ y_o \\ z_o \\ \dot{x}_o \\ \dot{y}_o \\ \dot{z}_o \end{Bmatrix} \tag{5-3}$$

An estimate for the needed initial conditions is derived from another method (in this case, from the resonance orbit estimates presented earlier), and the orbit resulting from this state vector is numerically integrated for one revolution about the central body. For

purposes of this study, one revolution is defined as the time at which the satellite returns to the x-y plane with x a positive value (i.e., the second crossing of the x-y plane). The conditions at this point are then compared to the desired boundary conditions, and the difference between the two state vectors (whose components are referred to as the "state error" values for the remainder of this paper) is used to modify the initial conditions. The specific method used in this modification depends on the details of the method used, as is outlined in the following sections. The new initial conditions are again integrated, and the process is repeated until the boundary condition is met, to within a specified numerical tolerance. In other words, the state error values are forced to be very small at the end of the program. An illustration of the process is provided in Figure 5-1.

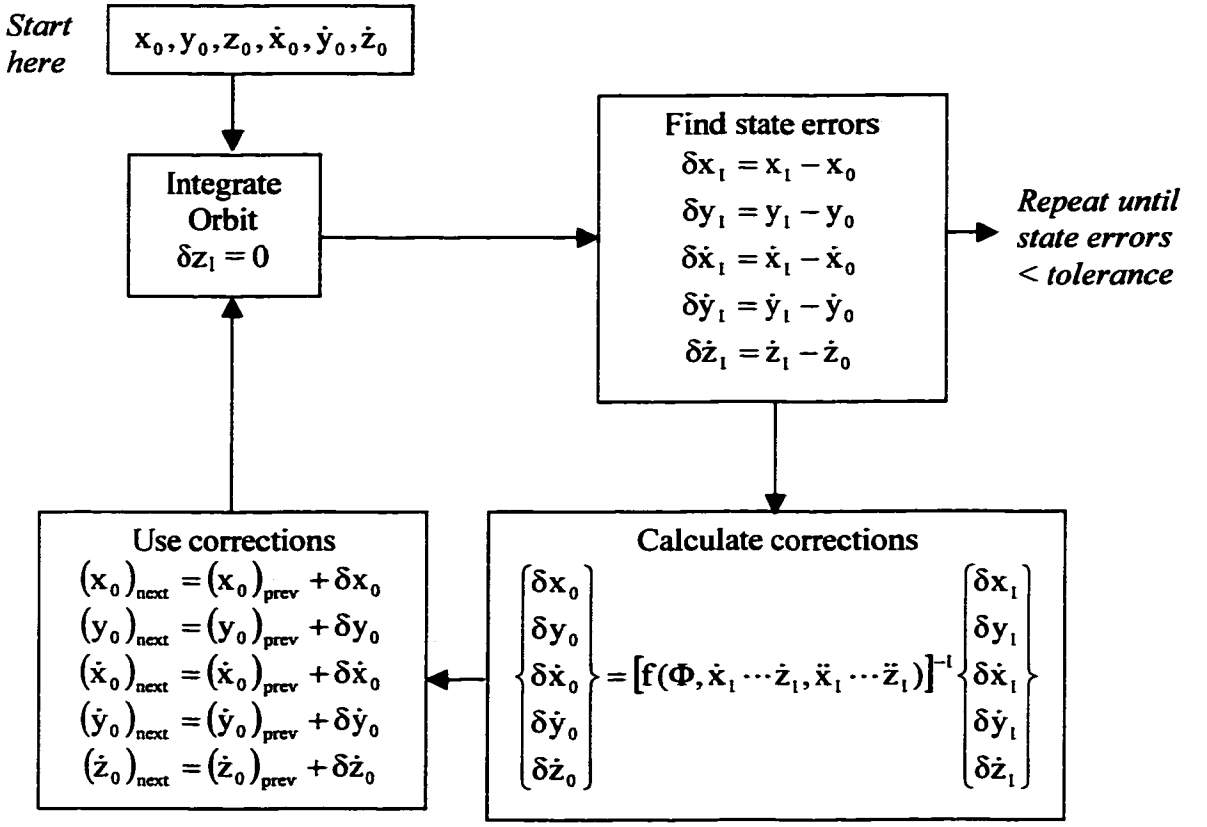

Figure 5-1. Differential Corrections Flowchart

For a specific orbit that converges to a solution, the state error values may fluctuate over the course of the differential corrections process, but one would expect the error values to decrease in absolute value as the algorithm proceeds. There is the possibility,

however, of the error values increasing in value, only to decrease later. The algorithm in this study includes a check of the maximum correction value. If the largest correction is greater than one nondimensional unit, the correction is stopped, and that case is considered to be non-convergent. The assumption is that, if the correction values are too large, the algorithm will likely not converge on a solution, and so no more computer time is used. This is a similar situation to that of a Newton-Raphson algorithm applied to a highly irregular function, so that an answer is never reached. A side issue would then be to study the size of the error values as functions of iteration to see if the algorithm appears to be converging.

When considering this type of problem, one needs to consider two kinds of ramifications. There are the practical concerns of orbiting an asteroid, for example, finding an orbit that neither crashes nor escapes, and achieving some optimal distance from the surface for maximum sensor efficiency. There are also concepts that are more purely mathematical in nature. For instance, in cases where the algorithm converges, can the tolerance be made as small as desired? Do starting estimates that are numerically close lead to the same solution? The methods presented in the next sections are tested under different asteroids, and with different orbit sizes in an attempt to answer these questions.

A. Method 1: 5x5 State Transition Matrix

The first differential correction method discussed utilizes a 5x5 state transition matrix. The initial values for the state variables are specified as

$$\begin{aligned} x_o &> 0 \\ y_o &= 0 \\ z_o &= 0 \\ \dot{x}_o &= 0 \\ \dot{y}_o &> 0 \\ \dot{z}_o &> 0 \end{aligned} \tag{5-4}$$

In this method, the error values of five of the state variables after one revolution $(x_1, y_1, \dot{x}_1, \dot{y}_1, \dot{z}_1)$ are controlled by modifying the corresponding initial values

$(x_0, y_0, \dot{x}_0, \dot{y}_0, \dot{z}_0)$. While y_o and $\dot{x}_o$ are set to zero at the beginning of this process, they will both be modified, and will in general be nonzero at the conclusion of the algorithm. One revolution is defined by the time necessary for the object to return to the x-y plane (i.e., $z_1 = 0$) with $x_1 > 0$, i.e., the second crossing of the x-y plane by the spacecraft. Additionally, z_0 is not modified. The changes in the initial state variables are given by

$$\begin{Bmatrix} \delta x_o \\ \delta y_o \\ \delta \dot{x}_o \\ \delta \dot{y}_o \\ \delta \dot{z}_o \end{Bmatrix} = B^{-1} \begin{Bmatrix} \delta x_1 \\ \delta y_1 \\ \delta \dot{x}_1 \\ \delta \dot{y}_1 \\ \delta \dot{z}_1 \end{Bmatrix} \tag{5-5}$$

where the 5x5 matrix B is derived from the differential correction matrix equation

$$\delta \bar{x}_1 = \Phi(t_1, t_0)\delta \bar{x}_0 + \frac{\partial \bar{x}_1}{\partial (t_1 - t_0)}\delta(t_1 - t_0) \tag{5-6}$$

Here Φ is the state transition matrix defined by $\frac{d\Phi(t, t_0)}{dt} = A\Phi(t, t_0)$ with $\Phi(t_0, t_0) = I$ and

$$A = \begin{bmatrix} 0 & 0 & 0 & 1 & 0 & 0 \\ 0 & 0 & 0 & 0 & 1 & 0 \\ 0 & 0 & 0 & 0 & 0 & 1 \\ V_{xx} & 0 & 0 & 0 & 2 & 0 \\ 0 & V_{yy} & 0 & -2 & 0 & 0 \\ 0 & 0 & V_{zz} & 0 & 0 & 0 \end{bmatrix} \tag{5-7}$$

The vectors $\bar{x}_0$ and $\bar{x}_1$ are the state vectors at the initial time step and at one revolution, respectively, that is $\bar{x}_0 = (x_0, y_0, z_0, \dot{x}_0, \dot{y}_0, \dot{z}_0)^T$ and $\bar{x}_1 = (x_1, y_1, z_1, \dot{x}_1, \dot{y}_1, \dot{z}_1)^T$. The state error vector $\delta \bar{x}_1$ gives, for each state variable, the difference between the actual value and the desired value. This vector is defined by

$$\delta\bar{x}_1 = \begin{Bmatrix} \delta x_1 \\ \delta y_1 \\ \delta z_1 \\ \delta \dot{x}_1 \\ \delta \dot{y}_1 \\ \delta \dot{z}_1 \end{Bmatrix} = \begin{Bmatrix} x_0 - x_1 \\ y_0 - y_1 \\ z_0 - z_1 \\ \dot{x}_0 - \dot{x}_1 \\ \dot{y}_0 - \dot{y}_1 \\ \dot{z}_0 - \dot{z}_1 \end{Bmatrix} \tag{5-8}$$

The correction vector $\delta\bar{x}_0$ gives the corrections that must be made to each state variable prior to the next iteration, that is

$$\delta\bar{x}_0 = \begin{Bmatrix} \delta x_0 \\ \delta y_0 \\ \delta z_0 \\ \delta \dot{x}_0 \\ \delta \dot{y}_0 \\ \delta \dot{z}_0 \end{Bmatrix} \tag{5-9}$$

and

$$\begin{aligned} (x_0)_{next} &= (x_0)_{prev} + \delta x_0 \\ (y_0)_{next} &= (y_0)_{prev} + \delta y_0 \\ (z_0)_{next} &= (z_0)_{prev} + \delta z_0 \\ (\dot{x}_0)_{next} &= (\dot{x}_0)_{prev} + \delta \dot{x}_0 \\ (\dot{y}_0)_{next} &= (\dot{y}_0)_{prev} + \delta \dot{y}_0 \\ (\dot{z}_0)_{next} &= (\dot{z}_0)_{prev} + \delta \dot{z}_0 \end{aligned} \tag{5-10}$$

Since the z-component of the state vector is used to define one revolution, the third row of Equation (5-6) is used to find $\delta(t_1 - t_0)$.

$$\delta z_1 = \Phi_{31}\delta x_0 + \Phi_{32}\delta y_0 + \Phi_{33}\delta z_0 + \Phi_{34}\delta \dot{x}_0 + \Phi_{35}\delta \dot{y}_0 + \Phi_{36}\delta \dot{z}_0 + \dot{z}_1\delta(t_1 - t_0) \tag{5-11}$$

The quantity δz_1 will be negligible, since the orbit is integrated until $z_1 = 0$ to within a small numerical tolerance, so δz_1 is assumed to be zero. In addition, since the initial z value is not changed in this process, $\delta z_0 = 0$ by definition. The state transition matrix Φ is integrated with the equations of motion. In this and all subsequent equations, Φ_{mn}

refers to the value in the m'th row and n'th column of the matrix Φ at one revolution $(t = t_1)$. We can then solve Equation (5-11) for $\delta(t_1 - t_0)$:

$$\delta(t_1 - t_0) = -\frac{1}{\dot{z}_1}(\Phi_{31}\delta x_0 + \Phi_{32}\delta y_0 + \Phi_{34}\delta \dot{x}_0 + \Phi_{35}\delta \dot{y}_0 + \Phi_{36}\delta \dot{z}_0) \tag{5-12}$$

This can be used to subsequently solve Equation (5-6) for the correction vector $\delta\bar{x}_0$. The third row of this matrix equation was already used and so is removed from the matrix. Similarly, since $\delta z_0 = 0$, the third column is also removed. This leaves a 5x5 matrix to be solved. The individual rows of this matrix are

$$\begin{aligned}
\delta x_1 &= \Phi_{11}\delta x_0 + \Phi_{12}\delta y_0 + \Phi_{14}\delta \dot{x}_0 + \Phi_{15}\delta \dot{y}_0 + \Phi_{16}\delta \dot{z}_0 + \dot{x}_1\delta(t_1 - t_0) \\
\delta y_1 &= \Phi_{21}\delta x_0 + \Phi_{22}\delta y_0 + \Phi_{24}\delta \dot{x}_0 + \Phi_{25}\delta \dot{y}_0 + \Phi_{26}\delta \dot{z}_0 + \dot{y}_1\delta(t_1 - t_0) \\
\delta \dot{x}_1 &= \Phi_{41}\delta x_0 + \Phi_{42}\delta y_0 + \Phi_{44}\delta \dot{x}_0 + \Phi_{45}\delta \dot{y}_0 + \Phi_{46}\delta \dot{z}_0 + \ddot{x}_1\delta(t_1 - t_0) \\
\delta \dot{y}_1 &= \Phi_{51}\delta x_0 + \Phi_{52}\delta y_0 + \Phi_{54}\delta \dot{x}_0 + \Phi_{55}\delta \dot{y}_0 + \Phi_{56}\delta \dot{z}_0 + \ddot{y}_1\delta(t_1 - t_0) \\
\delta \dot{z}_1 &= \Phi_{61}\delta x_0 + \Phi_{62}\delta y_0 + \Phi_{64}\delta \dot{x}_0 + \Phi_{65}\delta \dot{y}_0 + \Phi_{66}\delta \dot{z}_0 + \ddot{z}_1\delta(t_1 - t_0)
\end{aligned} \tag{5-13}$$

Equation (5-12) can be inserted into this equation, and the terms arranged to provide the matrix B necessary in Equation (5-5). The final matrix is shown in Equation (5-14).

$$B = \begin{bmatrix} \Phi_{11} & \Phi_{12} & \Phi_{14} & \Phi_{15} & \Phi_{16} \\ \Phi_{21} & \Phi_{22} & \Phi_{24} & \Phi_{25} & \Phi_{26} \\ \Phi_{41} & \Phi_{42} & \Phi_{44} & \Phi_{45} & \Phi_{46} \\ \Phi_{51} & \Phi_{52} & \Phi_{54} & \Phi_{55} & \Phi_{56} \\ \Phi_{61} & \Phi_{62} & \Phi_{64} & \Phi_{65} & \Phi_{66} \end{bmatrix} - \frac{1}{\dot{z}_1}\begin{Bmatrix} x_1 \\ y_1 \\ \dot{x}_1 \\ \dot{y}_1 \\ \dot{z}_1 \end{Bmatrix}\begin{bmatrix} \Phi_{31} & \Phi_{32} & \Phi_{34} & \Phi_{35} & \Phi_{36} \end{bmatrix} \tag{5-14}$$

B. Method 2: Derivative of Poincaré Map Algorithm

This method is similar to the 5x5 method, but the Jacobi integral of the system is used to keep the energy of the orbit constant. In this scenario, the initial z-component of the velocity is given as a function of the other initial conditions, and so it need not be calculated in the state transition matrix. This algorithm is based on the method presented in Reference [15].

The change in the Jacobi constant is constrained to be zero

$$(J_x)_0\delta x_0+(J_y)_0\delta y_0+(J_{\dot x})_0\delta\dot x_0+(J_{\dot y})_0\delta\dot y_0+(J_{\dot z})_0\delta\dot z_0=0 \tag{5-15}$$

where J_x, J_y, etc. denote the partial derivatives of the Jacobi constant, given in Reference [2] as

$$J=\frac{1}{2}\omega\left(x^2+y^2+z^2\right)-\frac{1}{2}\left(\dot x^2+\dot y^2+\dot z^2\right)-V \tag{5-16}$$

Here V is the gravitational potential of the system, given in Chapter II. The rotational velocity of the asteroid is ω. Care must be taken to use the proper units in this equation, or the proper multiples if the nondimensional equations of motion are used, with $\omega=1$.

Solving Equation (5-15) for $\delta\dot z_0$ leads to

$$\delta\dot z_0=\frac{1}{\dot z_0}\left(J_x(0)\delta x_0+J_y(0)\delta y_0+J_{\dot x}(0)\delta\dot x_0+J_{\dot y}(0)\delta\dot y_0+J_{\dot z}(0)\delta\dot z_0\right) \tag{5-17}$$

Using Equation (5-17), the change in the initial z velocity value can be found as a function of the changes in other initial conditions and so need not be calculated in the inversion of the state transition matrix. The remaining changes are calculated using Equation (5-18).

$$\begin{Bmatrix}x_o\\y_o\\\dot x_o\\\dot y_o\end{Bmatrix}=B^{-1}\begin{Bmatrix}x_1\\y_1\\\dot x_1\\\dot y_1\end{Bmatrix} \tag{5-18}$$

where

$$B=\begin{bmatrix}\Phi_{11}&\Phi_{12}&\Phi_{14}&\Phi_{15}\\\Phi_{21}&\Phi_{22}&\Phi_{24}&\Phi_{25}\\\Phi_{41}&\Phi_{42}&\Phi_{44}&\Phi_{45}\\\Phi_{51}&\Phi_{52}&\Phi_{54}&\Phi_{55}\end{bmatrix}-\frac{1}{\dot z_1}\begin{Bmatrix}x_1\\y_1\\\dot x_1\\\dot y_1\end{Bmatrix}\begin{bmatrix}\Phi_{31}&\Phi_{32}&\Phi_{34}&\Phi_{35}\end{bmatrix} \tag{5-19}$$

$$-\frac{1}{\dot z_0}\left[\begin{Bmatrix}\Phi_{16}\\\Phi_{26}\\\Phi_{46}\\\Phi_{56}\end{Bmatrix}-\frac{\Phi_{36}}{\dot z_1}\begin{Bmatrix}\dot x_1\\\dot y_1\\\ddot x_1\\\ddot y_1\end{Bmatrix}\right]\begin{bmatrix}J_x(0)&J_y(0)&J_{\dot x}(0)&J_{\dot y}(0)\end{bmatrix}$$

The change in $\dot z_0$ is then calculated using

$$\delta\dot{z}_0 = \frac{1}{\dot{z}_0}\begin{bmatrix} J_x(0) & J_y(0) & J_{\dot{x}}(0) & J_{\dot{y}}(0) \end{bmatrix}\begin{Bmatrix} \delta x_0 \\ \delta y_0 \\ \delta\dot{x}_0 \\ \delta\dot{y}_0 \end{Bmatrix} \tag{5-20}$$

C. Initial Estimate Conditioner

As an aid for convergence in the differential correction procedures, an initial estimate "conditioner" is used to force the initial orbit to be more closely periodic. Convergence is not guaranteed after this algorithm has been used, but in some cases convergence can be more easily facilitated, as will be shown. In this algorithm, the particle starts on the x-axis in a circular orbit. From there, two corrections are performed. First, the orbital radius is modified to force z_1 to be zero. Then the inclination is modified to force y_1 to be zero. Both of these corrections are performed using a secant method. For example, in the first correction, the orbit is propagated, and the orbital radius is modified according to

$$r_{n+1} = r_n - \frac{z_1}{S} \tag{5-21}$$

The sensitivity S is approximated using a finite difference method, hence making this a secant method. In order to calculate S, the orbit needs to be integrated twice. In the first integration, the radius "r" is decreased ($r_{prev} = 0.99\ r$) and the orbit is integrated for one revolution, with the resulting z_1 value denoted as $(z_1)_{prev}$. The integration time is kept constant and equal to the Keplerian estimate in this process. This is in contrast to the differential correction algorithm itself, where the integration time is allowed to change in order to meet the desired condition $z_1=z_0$. In the second integration, the radius is increased ($r_{next} = 1.01\ r$) and the orbit is again integrated, with the resultir.g z_1 value denoted as $(z_1)_{next}$. The sensitivity S is then calculated as

$$S = \frac{(z_1)_{next} - (z_1)_{prev}}{r_{next} - r_{prev}} \tag{5-22}$$

Once this value is calculated, it is used as the sensitivity throughout the remaining iterations. As the radius is modified, the resulting z_I value can be driven to a small numerical tolerance.

A similar method is used for the second correction, where the initial inclination is modified in order to drive y_I to zero. For this correction, the sensitivity is calculated as

$$S = \frac{(y_I)_{next} - (y_I)_{prev}}{i_{next} - i_{prev}} \tag{5-23}$$

where $i_{prev} = 0.99\ i$ and $i_{next} = 1.01\ i$, with i being the inclination of the original orbit.

The first correction is applied to the estimated initial conditions, and is iterated until the corresponding z_I error value is within the desired tolerance. Then the second correction is applied to the resulting initial conditions, and it is iterated until the corresponding y_I error value is within the desired tolerance. When the second correction is applied, z_I will, in most cases, be forced away from the nonzero condition attained in the first correction. However, in the cases shown here, the final values for both y_I and z_I are smaller than those of the initial estimate, so the method is successful in making the orbits closer to periodic, even though the final results are still not truly periodic. The differential correction algorithms are then used to force the orbits to meet the target condition of interest.

D. Results

Here the results of the initial estimate conditioner and the differential corrections algorithm are presented.

1. Initial Estimate Conditioner

Tables 5-1 through 5-4 show the results of the orbit conditioner for Gaspra, Eros, Ida, and Vesta, respectively. Each table lists the results for four resonance orbits with the estimated semimajor axis, (the eccentricity is set to zero, the inclination is set to 90° for all orbits) and the resulting semimajor axis and inclination after the conditioner has been run. In two cases, the 1:1 orbit for Ida and Eros, the orbit impacted the surface during the first revolution, so the algorithm did not integrate further. In the remaining cases, the

semimajor axes and the inclinations were varied only slightly in order to make the orbits more closely periodic. In all cases, the initial orbit was given a retrograde inclination (greater than 90°). This situation is analogous to frozen orbits about the Earth, in which the orbit is slightly retrograde to take advantage of the effect of Earth's oblateness.

Table 5-1. Gaspra Conditioned Orbits

Resonance	Estimated "r" (km)	Final "r" (km)	Final "i" (deg)
1:1	17.0228	17.2050	105.0997
2:1	27.0220	27.0270	90.6920
3:1	35.4088	35.4244	90.1170
4:1	42.8947	42.9108	90.0606

Table 5-2. Eros Conditioned Orbits

Resonance	Estimated "r" (km)	Final "r" (km)	Final "i" (deg)
1:1	20.0870	Orbit crashed	
2:1	31.8862	31.8932	93.6955
3:1	41.7827	41.8412	90.6635
4:1	50.6162	50.6865	90.2960

Table 5-3. Ida Conditioned Orbits

Resonance	Estimated "r" (km)	Final "r" (km)	Final "i" (deg)
1:1	28.9590	Orbit crashed	
2:1	45.9695	46.0049	93.1882
3:1	60.2370	60.3254	90.5836
4:1	72.9270	73.0722	90.2610

Table 5-4. Vesta Conditioned Orbits

Resonance	Estimated "r" (km)	Final "r" (km)	Final "i" (deg)
1:1	508.4787	510.0998	95.5451
2:1	807.1596	807.61348	90.1429
3:1	1057.6783	1058.07010	90.02077
4:1	1281.2860	1281.6229	90.0103

2. Differential Corrections

Tables 5-5 through 5-8 list the case studies that were performed for Gaspra, Eros, Ida, and Vesta, respectively. Of the four asteroids considered in this paper, Gaspra and Vesta were chosen as the primary objects of study since they are the most extreme in size. Since Vesta is the largest asteroid and Gaspra the smallest, one might assume that these two asteroids would have the most disparate qualities in terms of dynamics about them.

As the tables show, both Methods 1 and 2 had some success, but neither provided a solution in all cases. The orbits that converged on a solution did so within roughly 10,000 iterations, with the corrections smoothly approaching zero (with large increases in some cases). In some non-convergent cases, the corrections fluctuated quite irregularly and eventually exceeded the limit set in the program at which the algorithm terminated. In other cases that did not converge, the algorithm at first seemed to converge, until all error values were relatively small, but then all error values progressively increased in absolute value. Converged and non-converged cases are discussed below.

For some cases, a "convergence improvement factor" was required, in which the changes to the state variables at each iteration were multiplied by a small number (0.1 in all cases) in order to keep the algorithm from drastically changing the nature of the initial orbit. This is a common tactic in numerical analysis. The value to be used was arbitrarily chosen and has no real significance other than the ability to allow the algorithm to converge to a solution.

Table 5-5. Gaspra Case Studies

Case	Orbit	Method	Raw/Conditioned	Result
1	1:1	1	Raw	No convergence
2	1:1	1	Conditioned	No convergence
3	1:1	2	Raw	No convergence
4	1:1	2	Conditioned	Converged to 10^{-9} with convergence factor
5	2:1	1	Raw	No convergence
6	2:1	1	Conditioned	No convergence
7	2:1	2	Raw	No convergence
8	2:1	2	Conditioned	No convergence
9	3:1	1	Raw	Converged to 10^{-4}, then diverged, with convergence factor
10	4:1	1	Raw	Converged to 10^{-5} with convergence factor

Table 5-6. Vesta Case Studies

Case	Orbit	Method	Raw/Conditioned	Result
1	1:1	1	Raw	No convergence
2	1:1	1	Conditioned	No convergence
3	1:1	2	Raw	No convergence
4	1:1	2	Conditioned	Converged to 10^{-8}
5	2:1	1	Raw	No convergence
6	2:1	1	Conditioned	No convergence
7	2:1	2	Raw	No convergence
8	2:1	2	Conditioned	No convergence
9	3:1	1	Conditioned	Converged to 10^{-7}, then diverged

One orbit was successfully discovered for both asteroids, where convergence is defined as a case where all error values were driven to be 10^{-8} (in nondimensional units) or smaller in absolute value. Orbits were found near the 1:1 resonant conditions about Gaspra and Vesta. Discussions of specific results follow in the next sections.

i. Gaspra 1:1 Orbit

Figure 5-2 shows the progression of the differential corrections for the Gaspra 1:1 resonance orbit. The Poincaré method (with a convergence factor of 0.1) was applied to the conditioned initial state variables. The initial variables are shown in Table 5-7 in nondimensional (ND) units. The algorithm converged on a solution with all error values

less than 10^{-9} in absolute value (nondimensional) after 12,624 iterations. The error values for the first and final iterations are shown in Table 5-8.

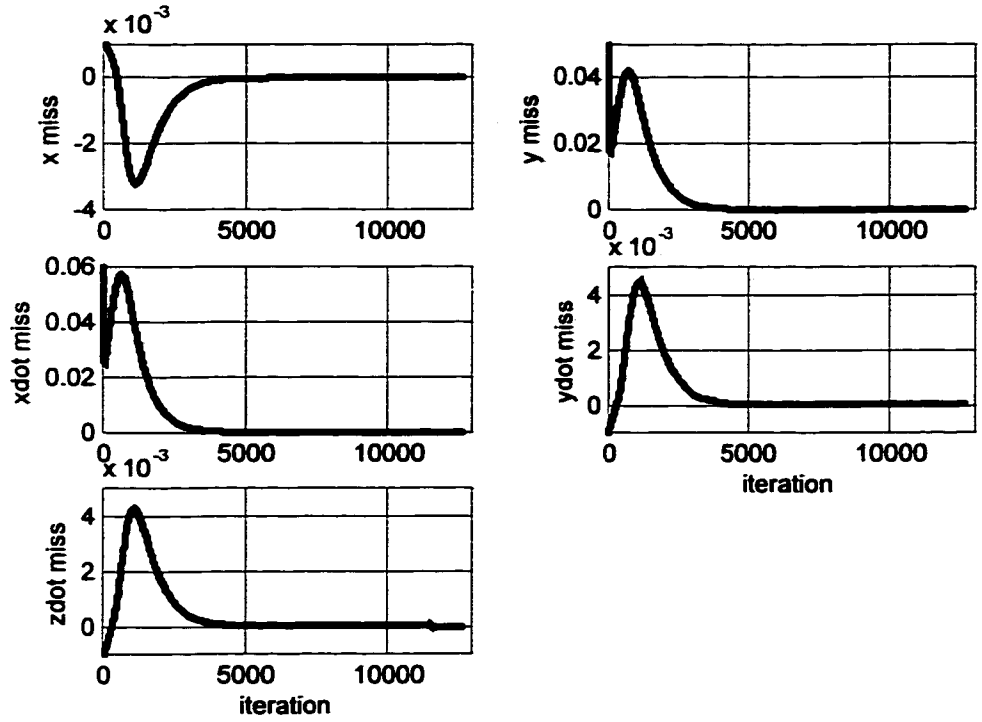

Figure 5-2. Differential Correction Progression for Gaspra 1:1 Orbit
Conditioned Orbit, using Poincaré method

Table 5-7. Gaspra 1:1 Resonance Orbit Estimated Initial Conditions
After Orbit Conditioner

State Variable	Initial Value (ND)	Initial Value (Dimensional)
x	1.811053	17.2050 km
y	0	0 km
z	0	0 km
$\dot{x}$	0	0 km/sec
$\dot{y}$	-2.282831	-0.0054072 km/sec
$\dot{z}$	1.750614	0.0041417 km/sec

Table 5-8. Error Values for Gaspra 1:1 Resonance Orbit

State Variable	Error Value, Iteration #1 (ND)	Error Value, Iteration #12,624 (ND)
x	-0.003	-1.9×10^{-10}
y	0.08	9.9×10^{-10}
$\dot{x}$	0.1	9.5×10^{-10}
$\dot{y}$	-0.003	2.5×10^{-10}
$\dot{z}$	0.0006	-9.0×10^{-10}

Table 5-9 shows the corrected initial conditions (i.e., the initial conditions after the differential corrections has been applied) in both nondimensional and dimensional form. Table 5-10 compares the orbital elements of the orbit before and after the differential corrections. In this case, the semimajor axis, eccentricity and inclination were all changed significantly.

Table 5-9. Gaspra 1:1 Resonance Orbit Corrected Initial Conditions
After Orbit Conditioner and Differential Corrections

State Variable	Initial Value (ND)	Initial Value (Dimensional)
x	1.568734	14.9030 km
y	-4.097859×10^{-9}	-3.89297×10^{-8} km
z	0	0
$\dot{x}$	-4.460396×10^{-9}	-1.05652×10^{-11} km/sec
$\dot{y}$	-0.995663	-0.0023584 km/sec
$\dot{z}$	2.041288	0.0048351 km/sec

Table 5-10. Gaspra 1:1 Orbit Before and After Differential Corrections

Orbital Element	Before Differential Corrections	After Differential Corrections
a (km)	17.825	19.247
e	0.0348	0.2257
i (deg)	105.083	74.318
ω (deg)	0	0
Ω (deg)	0	0
ν (deg)	0	0

ii. Vesta 1:1 Orbit

Figure 5-3 shows the progression of the differential corrections for the Vesta 1:1 resonance orbit. In this case, the Poincaré method was applied to the conditioned initial conditions (with the resulting state variables shown in Table 5-11), and the algorithm converged on a solution with all error values less than 10^{-8} in absolute value (nondimensional) after 1,581 iterations. The error values for the first and final iterations are shown in Table 5-12. The initial error values for the Vesta 1:1 orbit were much smaller than those for the Gaspra 1:1 orbit, so it would seem reasonable that the Vesta orbit would converge to a solution much more quickly than the Gaspra orbit. The resulting initial conditions, after the differential corrections program has been applied, are shown in Table 5-13. Table 5-14 compares the orbital elements of the orbit before and after the algorithm has been applied.

Table 5-11. Vesta 1:1 Resonance Orbit Estimated Initial Conditions
After Orbit Conditioner

State Variable	Initial Value (ND)	Initial Value (Dimensional)
x	1.924905	510.0998 km
y	0	0 km
z	0	0 km
$\dot{x}$	0	0 km/sec
$\dot{y}$	-2.110907	-0.184211 km/sec
$\dot{z}$	1.915897	0.167194 km/sec

Table 5-12. Error Values for Vesta 1:1 Resonance Orbit

State Variable	Error Value, Iteration #1 (ND)	Error Value, Iteration #1,581 (ND)
x	-1.4×10^{-5}	5.9×10^{-10}
y	5.9×10^{-4}	-5.6×10^{-9}
$\dot{x}$	6.4×10^{-4}	-7.5×10^{-9}
$\dot{y}$	5.7×10^{-6}	-1.0×10^{-9}
$\dot{z}$	6.8×10^{-6}	-3.1×10^{-9}

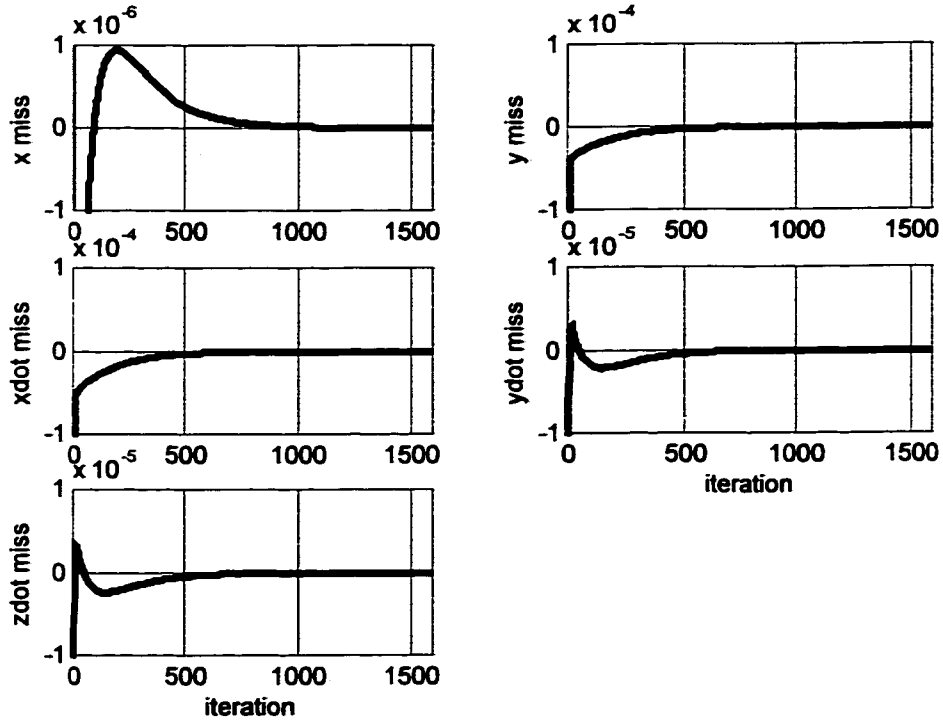

Figure 5-3. Differential Correction Progression for Vesta 1:1 Orbit
Conditioned Orbit, using Method #2

Table 5-13. Vesta 1:1 Resonance Orbit Corrected Initial Conditions
After Orbit Conditioner and Differential Corrections

State Variable	Initial Value (ND)	Initial Value (Dimensional)
x	1.925185	510.1739 km
y	-1.349825×10^{-7}	-3.57704×10^{-5} km
z	0	0
$\dot{x}$	-1.844190×10^{-7}	-1.60936×10^{-8} km/sec
$\dot{y}$	-2.112091	-0.184315 km/sec
$\dot{z}$	1.915497	0.167159 km/sec

Table 5-14. Vesta 1:1 Orbit Before and After Differential Corrections

Orbital Element	Before Differential Corrections	After Differential Corrections
a (km)	515.041	515.023
e	0.009595	0.009416
i (deg)	95.5451	95.5730°
ω (deg)	0	-0.004137°
Ω (deg)	0	-4.01724×10^{-5} °
ν (deg)	0	0.004137°

With the orbit now closely periodic, it is desirable to compare the orbits with the three sets of initial conditions: (1) the estimated elements derived from the Keplerian solution, (2) the elements after the orbit conditioner has been applied, and (3) the elements after the differential corrections algorithm has been applied. The orbit evolving from the estimated initial conditions is shown in Figure 5-4. This figure shows, relative to the inertial frame, the x-y projection of the orbit over the course of 40 days (roughly 180 revolutions). The orbit maintains its circular shape and also its initial size throughout this time period, but the orbit precesses significantly, achieving a node angle of 45° at the end of 40 days, producing a precession rate of 1.1 deg/day. Figure 5-5, by contrast, shows a similar plot for the orbit produced by the orbit conditioner. This orbit differs from the previous orbit in a number of ways. This orbit precesses in the opposite direction to that of the estimated orbit. This implies the existence of a "critical inclination" at which the precession is zero, and that this critical inclination is between these two orbits. In addition, the precession rate is much smaller for the second orbit. At the end of the time period, the node angle of this orbit is approximately 27°, giving a precession rate of 0.7 deg/day. Figure 5-6 shows the plot for the orbit produced by the differential corrections applied to the conditioned orbital elements. The precession rate of this orbit is even smaller, which is to be expected since the differential corrections program would produce an orbit with position and velocity after one revolution very close to the initial conditions. One would expect the precession rate to decrease as the error values decrease. For this orbit, the node angle is 12° after 40 days, giving a nodal rate of 0.3 deg/day.

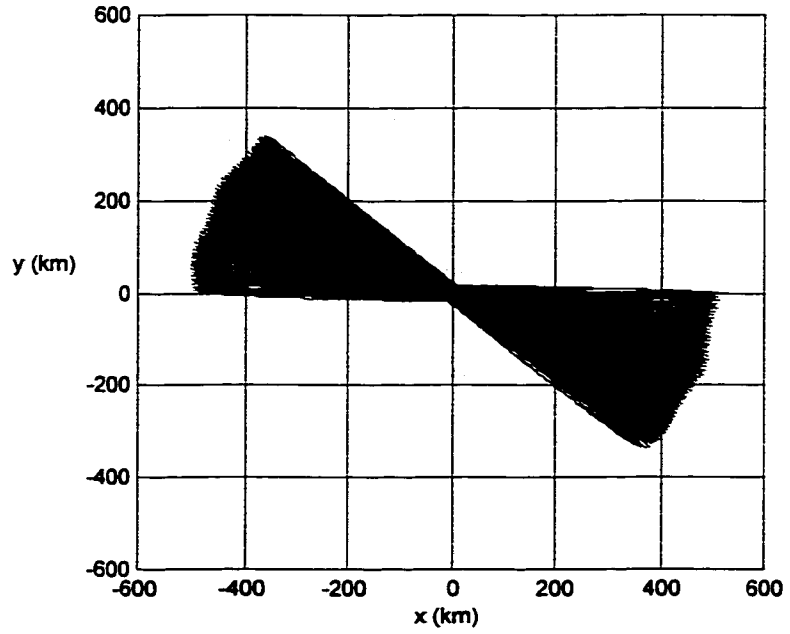

Figure 5-4. Inertial Frame Projection for Estimated Vesta 1:1 Orbit
40 days (roughly 180 revolutions) shown

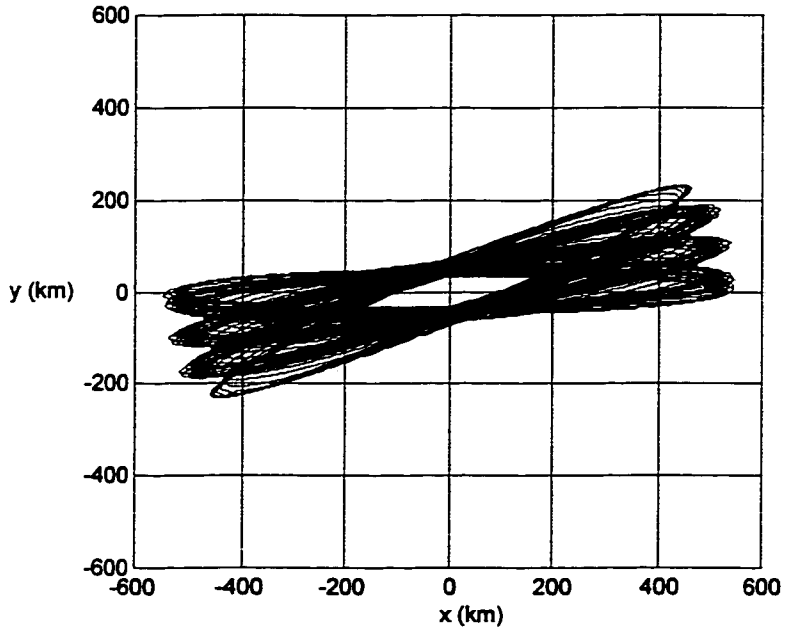

Figure 5-5. Inertial Frame Projection for Vesta 1:1 Orbit After Conditioner
40 days (roughly 180 revolutions) shown

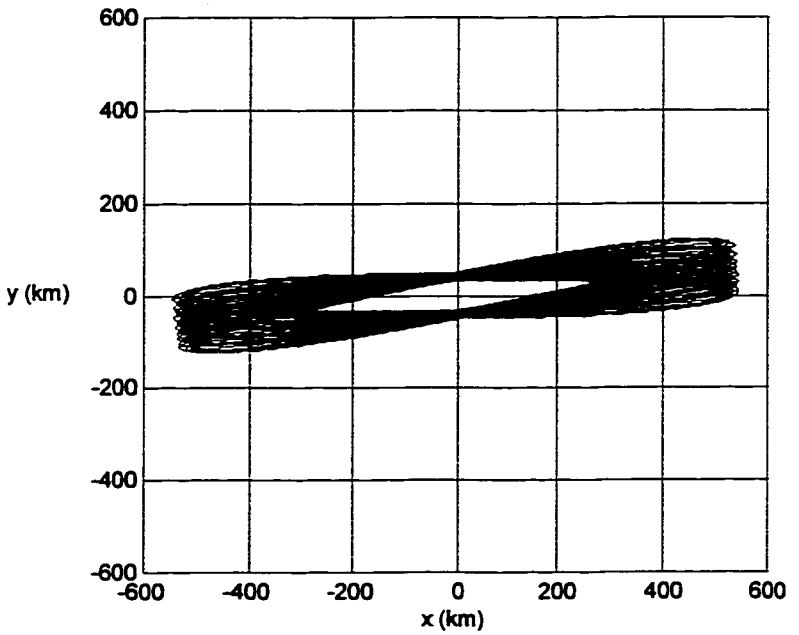

Figure 5-6. Inertial Frame Projection for Vesta 1:1 Orbit After Differential Corrections
40 days (roughly 180 revolutions) shown

iii. Vesta 3:1 Orbit

Figure 5-7 shows the progression of the differential correction algorithm for the conditioned Vesta 3:1 resonance orbit, using Method #1. No convergence factor was used in this case. This is an example of an initial estimate that appears to converge to a solution before slowly diverging. The state variables used for the initial estimate are shown in Table 5-15, and the error values are shown in Table 5-16. The minimum error magnitude, defined as the square root of the sum of the squares of the state error components (as shown in Equation (5-24)), occurs at iteration 1,711.

$$M = \sqrt{(\delta x_1)^2 + (\delta y_1)^2 + (\delta \dot{x}_1)^2 + (\delta \dot{y}_1)^2 + (\delta \dot{z}_1)^2} \tag{5-24}$$

The algorithm appears to converge to a solution, but then slowly diverges, with the error values becoming more significant. It is unclear whether this orbit would eventually converge upon another solution or simply "blow up," with the orbit possibly attaining a hyperbolic nature.

Table 5-15. Vesta 3:1 Resonance Orbit Initial Conditions
After Orbit Conditioner

State Variable	Initial Value (ND)
x	3.992717
y	0
z	0
$\dot{x}$	0
$\dot{y}$	-3.993200
$\dot{z}$	1.330905

Table 5-16. Error Values for Vesta 3:1 Resonance Orbit

State Variable	Error Value, Iteration #1	Error Value, Iteration #1,711 (Min. error magnitude, ND)	Error Value, Iteration #10,000 (ND)
x	1.0×10^{-7}	-2.9×10^{-8}	-7.7×10^{-8}
y	-2.6×10^{-6}	-1.7×10^{-8}	-5.3×10^{-6}
$\dot{x}$	2.1×10^{-6}	2.9×10^{-8}	-5.3×10^{-6}
$\dot{y}$	-1.0×10^{-7}	2.9×10^{-8}	7.4×10^{-8}
$\dot{z}$	-3.6×10^{-8}	4.4×10^{-9}	-2.4×10^{-10}

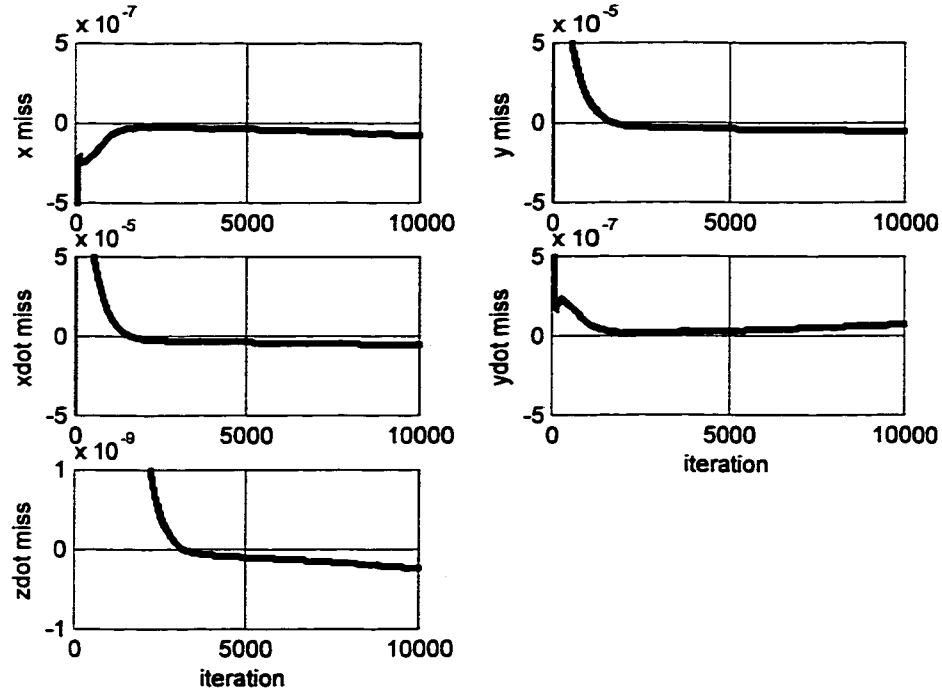

Figure 5-7. Differential Correction Progression for Vesta 3:1 Orbit
Conditioned Orbit, using Method #1

Table 5-17 shows the resulting initial conditions from the differential correction algorithm, both in nondimensional and dimensional form. Small nonzero values have been added to the y and $\dot{x}$ values. Table 5-18 compares the orbital elements of the orbit before and after the algorithm has been applied. None of the orbital elements were modified significantly in this case.

Table 5-17. Vesta 3:1 Resonance Orbit Corrected Initial Conditions
After Orbit Conditioner and Differential Corrections, at Iteration 1,711

State Variable	Initial Value (ND)	Initial Value (Dimensional)
x	3.991795	1057.816 km
y	-0.006113223	-1.6200 km
z	0	0
$\dot{x}$	-0.006117445	-5.33848×10^{-4} km/sec
$\dot{y}$	-3.992780	-0.348436 km/sec
$\dot{z}$	1.331225	0.116171 km/sec

Table 5-18. Vesta 3:1 Orbit Before and After Differential Corrections

Orbital Element	Before Differential Corrections	After Differential Corrections
a (km)	1059.248	1059.251
e	0.001112	0.001354
i (deg)	90.0208	90.0439
ω (deg)	0	0
Ω (deg)	0	0
ν (deg)	0	0

iv. Non-Converged Orbits

While there were some successful cases, there were a number of cases that did not converge to a solution despite the numerical "tricks" that were attempted. There are a number of possible explanations. In some cases, the small difference between the unconditioned and conditioned state variables was enough to allow convergence of a solution. In the case of the Vesta 1:1 orbit, the largest difference between the unconditioned and conditioned state variables was in $\dot{y}_0$, which was changed from –1.92

to –2.11 (nondimensional) by the orbit conditioner. The magnitudes of the changes in the other state variables are on the order of 0.01. The unconditioned state variables did not converge to a solution, while the conditioned variables did. This shows that a small change in the initial conditions can have a large effect on the convergence properties of the orbit.

It should not be assumed that no usable orbits exist in the regions where convergence was not attained. It may simply be a limitation of the method used, for any of the reasons listed above. One future objective remaining in this project would be to develop new methods for obtaining better initial conditions. New differential correction methods may be developed as well. The two methods presented here are both linear in nature. Higher-order methods may prove more robust in their ability to converge upon a solution without the necessity of starting very close to the final solution.

Chapter VI

Conclusions and Recommendations

The purpose of this study was to investigate periodic orbits about ellipsoidal shaped bodies in order to develop methods for use with asteroid and comet mission design. The background information necessary, including the equations of motion using elliptic integrals and harmonic coefficient expansion, is shown in Chapter II. These equations had been used in previous studies for a number of applications. The motivation of this study was to expand upon those efforts. The equilibrium points are also shown, and can be used as an initial tool to understand the dynamics about such bodies. Lagrange's Planetary Equations are also presented in Chapter II. These had been used in previous studies as well. New material presented in Chapter II includes the derivation of the equations of motion with solar gravity included (which is a detailed expansion of methods used in other studies), a derivation of the harmonic coefficients of ellipsoidal shaped bodies, and the definition for altitude used in this study. Chapter III presents the numerical parametric studies that were performed, where the properties of a large number of orbits were studied using phase plots of eccentricity and argument of periapsis, and also variations of the orbital elements as functions of initial semimajor axis. Some specific regions about the asteroids in question appear to have large changes in orbital elements over the course of the thirty days for which the orbits were integrated. These points appear to be near resonance points. Resonance is further discussed in Chapter IV, where plots of the rate of change of periapsis distance as a function of mean anomaly (i.e., dr_p/dM) are shown. Lagrange's Planetary Equations were used to derive this quantity. Of course, these methods still do not provide perfectly periodic orbits about asteroids. In Chapter V, two differential correction algorithms are described for use on orbits near resonance points in order to compute periodic orbits. While resonance points appeared to have adverse effects on orbits as shown in Chapter III, they can also have beneficial qualities. Since the ratio of the orbit period to rotational period of the asteroid is a small integer (1:1, 2:1, 3:1, and 4:1 in this study), this gives the reference frames symmetry in that one orbit revolution of the satellite corresponds to an integral number of

rotations of the asteroid. This means that the rotating and inertial reference frames coincide at the beginning of the orbit and also after one orbit revolution. This occurrence is useful in the method developed to seek periodic orbits.

The differential correction methods presented here were partially successful, converging on solutions in some cases, while convergence was not achieved in others. Orbits were found near the 1:1 resonance conditions of both Gaspra and Vesta. For these orbits, error values at one revolution were driven to small tolerances. The results are not truly periodic, However, they are much closer to being periodic than those given by the Keplerian estimate for the orbit size. This then provides a method for searching for periodic orbits about any asteroid. The algorithm is initialized with the Keplerian estimate for the size given the period, determined by the rotational rate of the asteroid and the resonance ratio. Those initial conditions are then used as an initial estimate in one or more differential correction algorithms, in conjunction with the orbit conditioner scheme if necessary. A convergence factor may also be used, where the correction values at each step are multiplied by a small number to keep the corrections from attaining large values, possibly forcing the orbit to become either hyperbolic or small enough that the satellite crashes into the surface. This was necessary in some cases, but not required in others.

An attempt is made to correlate the results from the different studies presented here (parametric studies, phase plots and parametric plots), in order to understand reasons for the cases that did not converge in the differential corrections programs. There appears to be no obvious and definite connection, however. In one case where the differential corrections converged (Vesta 1:1), the periapsis plots have no asymptotes present, unlike the plots for the Gaspra 2:1 and 4:1 orbits. On the other hand, the periapsis plot for the Gaspra 3:1 orbit has no asymptotes, yet the differential correction scheme did not converge. More combinations of orbits need to be run in the corrections program in conjunction with the periapsis plots to fully develop any correlation. The parametric studies and phase plots showed that resonance orbits can be quite erratic. This did not prevent the orbits from converging onto a solution. In fact, as stated previously, resonance orbits facilitate the search for polar orbits by nature of the reference frames

coinciding after one satellite revolution. As shown in Chapter III, the resonance orbits used here can have large changes in orbital elements over time. In addition, the periapsis plots show large changes in the rate of change of the periapsis distance, and in some cases this value approaches infinity. These effects can negate the positive effect of choosing a resonance orbit and the symmetry it provides for the reference frames.

There are a number of issues to be dealt with in future additions to this work,:

1. An improved force model can be developed. One example of the equations of motion for the Sun-asteroid-satellite three-body problem is shown in Chapter II. This can be expanded to include the gravity of Jupiter, an asymmetric shaped asteroid, a non-constant spin vector, solar radiation pressure, and other perturbations.
2. An improved differential correction scheme can be designed and implemented. A program that converges upon its solution in fewer iterations would be advantageous, requiring much less computer time to execute. In addition, a method that is not as sensitive to changes in the initial estimate would be useful. An algorithm that keeps the orbit period constant throughout the iterative process may assist in these goals.
3. For use in actual mission design, a rigorous study of the stability properties of the orbits in question should be performed. While some general qualitative comments can be made about the stability of the orbits shown here, no definite conclusions can be reached without such a study.
4. A stationkeeping and/or navigation scheme can be investigated, with the goal of deriving the ΔV budget for the mission in question. A perfectly periodic orbit would have no stationkeeping requirements, since the orbit would repeat *ad infinitum*. However, the orbits developed in this study do not meet this requirement exactly, hence requiring a stationkeeping analysis.
5. Finally, a calculation of the viewable surface of the central body would be useful. Polar orbits were chosen in this study to allow viewing of the entire surface, including the poles. A calculation of the viewable area, in conjunction with the

altitude definition shown in Chapter II, would provide invaluable data for mission analysis.

REFERENCES

1 German, D., and Friedlander, A. L., "A Simulation of Orbits Around Asteroids Using Potential Field Modeling," Proceedings of the AAS/AIAA Spaceflight Mechanics Meeting, Houston, TX, February 11-13, 1991.

2 Scheeres, D. J., "Dynamics about Uniformly Rotating Triaxial Ellipsoids: Applications to Asteroids," *Icarus*, 110 (1994): 225-238.

3 Chauvineau, B., Farinella, P., and Mignard, F., "Planar Orbits about a Triaxial Body: Application to Asteroidal Satellites," *Icarus*, 105 (1993): 370-384.

4 Chauvineau, B., and Mignard, F., "Dynamics of Binary Asteroids. I. Hill's Case," *Icarus*, 83 (1990): 360-381.

5 Hamilton, D. P., and Burns, J. A., "Orbital Stability Zones about Asteroids," *Icarus*, 92 (1991): 118-131.

6 Zhang, S.-P., and Innanen, K. A., "The Stable Region of Satellites of Large Asteroids," *Icarus*, 75 (1988): 105-112.

7 Chauvineau, B., and Mignard, F., "Dynamics of Binary Asteroids. II. Jovian Perturbations," *Icarus*, 87 (1990): 377-390.

8 Chauvineau, B., Mignard, F. and Farinella, P., "The Lifetime of Binary Asteroids vs. Gravitational Encounters and Collisions," *Icarus*, 94 (1991): 299-310.

9 Utashima, M., "Spacecraft Orbits Around Asteroids for Global Mapping," *Journal of Spacecraft and Rockets*, 34, No. 2 (1997): 226-232.

10 Scheeres, D. J., "Analysis of Orbital Motion Around 433 Eros," *The Journal of the Astronautical Sciences*, 43, No. 4, (October-December 1995): 427-452.

11 Kaula, W. M., *Theory of Satellite Geodesy*, Waltham, MA: Blaisdell Publishing Company, 1966, pp. 30-37.

12 MacMillan, W. D., *The Theory of the Potential*, New York: McGraw-Hill, 1930, pp. 56-60.

13 Battin, R. H., *An Introduction to the Mathematics and Methods of Astrodynamics*, New York: AIAA, 1987, pp. 68-78.

14 Rosborough, G., and Ocampo, C., "Influence of Higher Degree Zonals on the Frozen Orbit Geometry", AAS Paper 91-428, 1991.

15 Scheeres, D. J., "Satellite Dynamics About Tri-Axial Ellipsoids", presented at the Advances in Non-Linear Astrodynamics Conference, Minneapolis, Minnesota: University of Minnesota, November 8-10, 1993.